ACS Catalysis

Perspective

Cite This: ACS Catal. 2019, 9, 5912−5928

pubs.acs.org/acscatalysis

Oxidative Coupling of Methane (OCM) by SiO_2-Supported Tungsten Oxide Catalysts Promoted with Mn and Na

Daniyal Kiani,[‡] Sagar Sourav,[‡] Jonas Baltrusaitis,* and Israel E. Wachs*

Department of Chemical & Biomolecular Engineering, Lehigh University, Bethlehem, Pennsylvania 18015, United States

ABSTRACT: The literature for the oxidative coupling of methane (OCM) on supported $Mn/Na_2WO_4/SiO_2$ catalysts is systematically and critically reviewed. The influence of the precursors, starting SiO_2 support crystallinity, synthesis method, calcination temperature, and OCM reaction conditions on the catalyst structure is examined. The supported $Mn/Na_2WO_4/SiO_2$ catalyst system is found to be dynamic with the catalyst structure quite dependent on the set of variables. Although almost all of the reported studies have determined the catalyst crystalline structures under ambient conditions (room temperature and air exposed), recent in situ/operando characterization study under OCM reaction conditions revealed that all previously detected crystalline phases of the active Mn−Na−W−O components are not present because the reaction temperature is above the melting points of their oxides. The presence of Na also induces the crystallization of the silica support to SiO_2 (cristobalite) at elevated temperatures. The nature of the surface active sites under OCM reaction conditions is still not known because of the absence of in situ/operando surface spectroscopy characterization studies under relevant reaction conditions. Consequently, the proposed structure−activity models in the literature are highly speculative since they are lacking supporting data. The rate-determining-step involves activation of the methane C−H bond by atomic surface O* as demonstrated by a kinetic isotope effect (KIE) between CH_4 and CD_4. Although the reaction kinetics follow a Langmuir−Hinshelwood type mechanism, $r = [CH_4]^1[O_2]^{1/2}$, isotopic $^{18}O_2$−$^{16}O_2$ studies have shown that the catalyst lattice also provides O* for the OCM reaction suggesting involvement of a Mars−van Krevelen mechanism. Recommendations are given regarding the experimental investigations that could establish the fundamental reaction aspects of OCM by supported $Mn/Na_2WO_4/SiO_2$ catalysts that would allow for the rational design of improved catalysts.

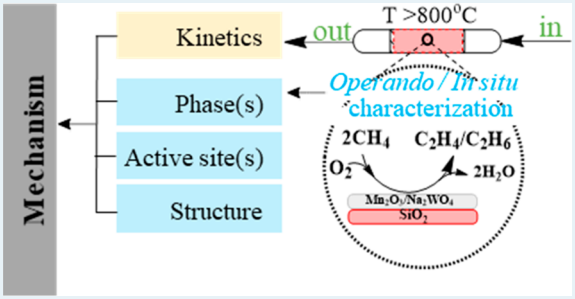

KEYWORDS: *methane, oxidative coupling, OCM, catalysts, $Mn/Na_2WO_4/SiO_2$, active sites*

1. INTRODUCTION

Despite increasingly strict regulations, a significant number of countries, such as USA, Russia, Nigeria, Iran, Iraq, and Saudi Arabia, still flare natural gas (mostly consisting of CH_4), which is estimated to be ∼30% of the total natural gas utilized in the world.[1] Moreover, shale gas, the natural gas accumulated in shale formations, has gained attention as a new source of energy and petrochemicals, especially in the USA. According to the recent statistics, shale gas production increased ∼500% from 2007 to 2013.[2] Unfortunately, most of these newfound reserves are stranded in difficult to access terrain that makes transportation of natural gas over long distances economically challenging.[3] Despite the vast availability of natural gas, CH_4 is underutilized as a chemical feedstock because of the dearth of direct methods to convert natural gas to value-added products. This recent abundance of natural gas (primarily from shale) has renewed interest in catalytic methods to convert natural gas to value-added chemicals. Natural gas can be converted to chemicals and fuels via *indirect* capital intensive routes by conversion to syngas (CO/H_2), which can be converted to fuels via the well-established catalytic Fischer−Tropsch synthesis (FTS) technology.[3] Alternatively, syngas can be initially catalytically converted to methanol that can be catalytically processed to small olefins (MTO = methanol to olefins), aromatics (MTA = methanol to aromatics), or gasoline (MTG = methanol to gasoline).[4]

The CH_4 can also be converted *directly* to value-added chemicals and fuels via oxidative and nonoxidative catalytic reaction routes. The nonoxidative processes involve coupling of CH_4 (NOCM) to olefins, aromatics, and hydrogen (MTOAH)[3] or CH_4 dehydroaromatization to benzene and H_2 (MDHA).[3,5] The nonoxidative routes, however, suffer from intrinsic thermodynamic limitations and require extremely high energy inputs rendering them challenging technologies for large scale application.[1,3,6−9] In contrast, the oxidative coupling of CH_4 (OCM) is not constrained by thermodynamic limitations and directly converts CH_4 to high-value chemicals, such as C_2H_6 and C_2H_4, with C_2H_4 representing ∼50% of the hydrocarbon feedstock for the chemical industry.[10] The OCM catalytic reaction was first reported by Keller and Bhasin in 1982[11] and has attracted significant attention over the years in order to gain a deeper understanding of its fundamentals with

Received: April 17, 2019
Revised: May 21, 2019
Published: May 22, 2019

DOI: 10.1021/acscatal.9b01585
ACS Catal. 2019, 9, 5912−5928

Table 1. Synthesis Methods and the Corresponding Crystalline Bulk Phases Identified with XRD for the Supported $Mn_xO_y/Na_2WO_4/SiO_2$ Catalysts

method	typical precursor and solvent	major bulk phases identified	refs
incipient-wetness impregnation (IWI)	$Mn(NO_3)_2$ and Na_2WO_4 in H_2O sometimes $Mn(CH_3COO)_2{\cdot}4H_2O$ is used too	Mn_2O_3, Na_2WO_4, WO_3, $MnWO_4$, SiO_2 (α-cristobalite)	13, 26, 31, 49, 54, 55, 60
mixed slurry (MS)	$Mn(NO_3)_2$ and Na_2WO_4 in H_2O	Mn_2O_3, Na_2WO_4, WO_3, $MnWO_4$, SiO_2 (α-cristobalite)	31, 49
sol−gel (SG)	$(C_2H_5)_4SiO_4$ in C_2H_5OH and HNO_3	Mn_2O_3, Na_2WO_4, $MnMn_6SiO_{12}$, SiO_2 (α-cristobalite), SiO_2 (tridymite), SiO_2 (quartz)	31, 60
physical mixing/ball milling (PM/BM)	$Mn(NO_3)_2$ and Na_2WO_4	Na_2WO_4, Mn_2O_3, SiO_2 (α-cristobalite)	13, 61, 62
polyhedral oligomeric silsesquioxanes (POSS)	$(C_4H_9)_7Si_7O_9(OH)O_2Mn$ and $(C_4H_9)_7Si_7O_{12}W$ and $(C_4H_9)_7Si_7O_9(OH)_2ONa$) in hexane−toluene	Mn_2O_3, Na_2WO_4, SiO_2 (α-cristobalite and tridymite).	49
fluidized bed processing (FP)	$Mn(NO_3)_2{\cdot}4H_2O$ and of $Na_2WO_4{\cdot}2H_2O$ in H_2O	Mn_2O_3, Na_2WO_4, SiO_2 (α-cristobalite), $MnWO_4$ (only in spent catalyst)	63, 64
solution combustion (SC)	$Mn(NO_3)_2$ and Na_2WO_4 in $C_8H_{20}O_4Si$ was the precursor for Si, as well as fuel	Na_2WO_4, Mn_2O_3, SiO_2 (α-cristobalite)	65
flame spray pyrolysis (FS)	W-ethoxide, Mn-2-ethylhexanoate, Na-2-ethylhexanoate and hexamethyldisiloxane in xylene	Na_2WO_4, SiO_2 (α-cristobalite), $MnWO_4$ (only in Na-free catalyst) Mn_2O_3 (only in spent catalyst)	66

the aim of making the OCM catalytic process commercially viable. Although OCM is not thermodynamically limited because the overall reaction is exothermic and exergonic, it is kinetically hindered and still needs better performing catalysts to make OCM industrially viable.[3,12] The OCM catalytic reaction faces selectivity issues since the free energy change of the OCM reaction is ∼−154 kJ/mol at 800 °C[3] while that of complete oxidation of CH_4 into CO_2 is ∼−801 kJ/mol.[3] In addition, the OCM catalytic process involves both heterogeneous and homogeneous reaction steps that further complicate its understanding.[13] Fundamentally, the process involves the activation of a C−H bond of CH_4 to form gaseous methyl radicals (CH_3•) via a heterogeneous catalytic step followed by a gas phase homogeneous recombination step of the CH_3• radicals to yield C_2H_6.[1,8,13−18] The C_2H_6 can further undergo oxidative dehydrogenation over the same catalyst to form the highly desired C_2H_4 product.[13] It has been reported that OCM holds the greatest potential as the most cost-effective and environmentally friendly method of converting CH_4 to chemicals compared to the energy and capital intensive indirect routes.[1]

This Perspective will focus only on the catalytic OCM reaction and the details of other CH_4 catalytic conversion processes can be found elsewhere in the literature.[1,19−22] The current review specifically focuses on the heterogeneous catalytic step of the OCM reaction involving activation of the CH_4 molecule to generate CH_3• radicals. Hundreds of catalysts (consisting of Group I, II, and transition metal oxides) have been examined for the OCM reaction to find catalysts with high C_2H_4 selectivity and suppression of overoxidation to carbon oxides (CO_x).[12,14,22,23] Although lithium (Li) in Li/MgO catalyst acts as a structural promoter for enhancing OCM performance through Li migration to the surface,[24,25] it suffers from intrinsic instability because of its excessive loss, over time, at the high reaction temperatures.[26,27] Lanthanum (La)-based catalysts, however, exhibit better thermal stability but suffer from selectivity issues.[22,23] The supported $Mn/Na_2WO_4/SiO_2$ catalyst is currently the only catalyst system that shows promising stability over long periods of operation under OCM conditions and exhibits CH_4 yields of ∼30% (conversion of ∼35% and C_2 selectivity of ∼80%).[12] Although many reviews have summarized the extensive OCM literature from the almost past four decades, most of them are either outdated or lack critical fundamental analysis of the literature data and just summarize the literature findings.[20,28−31] One of the most comprehensive reviews on the supported $Mn/Na_2WO_4/SiO_2$ catalyst system appeared in 2011 by Arndt et al.,[12] but this review lacked detailed discussion of OCM reaction kinetics studies and did not cover catalytic fundamentals (e.g., catalytic active sites, etc.). The aim of the current Perspective is to critically analyze the major literature studies regarding characterization of the catalyst structure, OCM kinetics, reaction mechanism, and proposed structure−activity models for OCM by the supported $Mn/Na_2WO_4/SiO_2$ catalyst with an emphasis on the catalyst structure. The influence of precursors, type of SiO_2 support, synthesis method, calcination temperature, and reaction conditions upon the catalyst structure is extensively examined, but mostly from ex situ techniques, since in situ and operando characterization studies are almost completely missing from the literature.[4,13,40−46,32−39] Through a systematic analysis of the catalytic OCM literature, a clearer picture of the current basic understanding of OCM by supported $Mn/Na_2WO_4/SiO_2$ catalysts is obtained and recommendations are made for future fundamental studies to advance this catalytic system that will be of great value for researchers in this field.

2. SYNTHESIS AND CHARACTERIZATION

The numerous synthesis methods reported for preparing supported $Mn/Na_2WO_4/SiO_2$ catalysts are summarized in Table 1. As precursors of the active components, aqueous soluble inorganic salts such as $Na_2WO_4{\cdot}2H_2O$, $Mn(NO_3)_2{\cdot}4H_2O$, $NaNO_3$, $(NH_4)_{10}(H_2W_{12}O_{42}){\cdot}4H_2O$, $C_2H_3NaO_2$, etc., have typically been employed. In some cases, special organic−inorganic precursors such as $(C_4H_9)_7Si_7O_9(OH)O_2Mn$ and $(C_4H_9)_7Si_7O_{12}W$ and $(C_4H_9)_7Si_7O_9(OH)_2ONa$) in hexane−toluene solvent mixtures were also employed. Significant variations can be seen in the nature and dispersion of the supported active phases with different precursors, solvents, type of SiO_2 support[47] and preparation methods that lead to diverse catalyst activity and stability properties.[48−53]

Prior to discussing the effect of using different synthesis methods in further detail, it is important to initially highlight the effect of the precursor on the final catalyst, irrespective of the synthesis techniques used. Typically, the incipient-wetness impregnation (IWI) method has been used for synthesizing the OCM catalysts under discussion, as it is simpler than some of the more technologically and economically demanding synthesis methods discussed in the later sections of this review. A scrutiny of the precursors used with the IWI synthesis method,

DOI: 10.1021/acscatal.9b01585
ACS Catal. 2019, 9, 5912−5928

Table 2. Summary of Synthesis, Characterization Techniques, and Experimental Conditions for OCM Catalysts

ref	catalyst synthesis	characterization techniques	phases detected
14	incipient-wetness impregnation of SiO_2 gel (Davison 57-08-5) with aqueous $Mn(NO_3)_2$ and Na_2WO_4 at 85 °C dried at 130 °C for 4−8 h; calcined in air at 800 °C for 8 h	XRD: Cu K_α (ambient) XPS: Mg K_α (UHV). LEIS: $3He^+$ ions, 134.5°, 1 kV (UHV) catalyst treated with CH_4:O_2 OCM stoichiometric ratio at 800 °C and transferred to UHV for analysis	SiO_2 (α-cristobalite and tridymite), Na_2WO_4, $MnWO_4$, Mn_7SiO_{12}, Mn_2O_3, $Na_2Si_2O_5$
58	incipient-wetness impregnation of SiO_2 gel with aqueous $Na_2C_2O_4$, $(NH_4)_5H_7(WO_4)_6$, Na_2WO_4, and $Mn(NO_3)_2$ at 90 °C air-dried at 120 °C, calcined in air at 830−850 °C for 6 h	XRD: Cu K_α (ambient) XPS: Mg K_α (UHV) fresh catalysts treated at 800 °C in O_2 for 30 min prior to analysis; spent catalysts de-gassed at room temperature in the pretreatment chamber Raman: 514.5 nm (ambient)	XRD showed Na_2WO_4, $Na_2W_2O_7$, $MnWO_4$, and (α-cristobalite) Raman showed bands at 900−950 cm^{-1} in pre- and post-OCM catalysts, which the authors did not explain well
26	Na_2WO_4/SiO_2: incipient-wetness impregnation of aqueous Na_2WO_4 onto SiO_2 gel at 90 °C, dried at 120 °C and calcined in air at 800 °C for 4 h WO_3/SiO_2: incipient-wetness impregnation of aqueous ammonium para-tungstate onto SiO_2 gel at 90 °C, dried at 120 °C and calcined in air at 800 °C for 4 h Na-WO_3/SiO_2: needed a second impregnation of calcined WO_3/SiO_2 with $NaNO_3$, dried at 120 °C and calcined in air at 800 °C for 4 h	XRD: Cu K_α (ambient) Raman: 532 nm (ambient)	Na_2WO_4, WO_3, SiO_2 (α-cristobalite)
56	prepared from aqueous slurry mixture of stoichiometric $Mn(NO_3)_2$ and Na_2WO_4 with SiO_2 gel, dried at 120 °C, calcined in air at 750−950 °C for 8 h	XRD: Cu K_α (ambient) XPS: Mg K_α (UHV) catalysts pretreated at 400 °C, 10^{-4} Torr and subsequently in the ultrahigh vacuum (UHV) chamber at 700 °C at 5×10^{-5} Torr PASCA (positron annihilation spectroscopy for chemical analysis): ^{22}Na	Na_2WO_4, Mn_2O_3, SiO_2 (α-cristobalite) for Na_2WO_4 loading >4%
57, 75	incipient-wetness impregnation of SiO_2 (140m^2/g) with aqueous Na_2WO_4 and $Mn(NO_3)_2$, dried at 120 °C and calcined in air at 800 °C for 4 h	Raman: 532 nm (pseudo in situ) EPR: vacuum at −198 °C catalyst oxidized at 780 °C for 30 min under 66.7 kPa O_2, followed by evacuation at same temperature	Na_2WO_4, Mn_2O_3, SiO_2 (α-cristobalite)
54	incipient-wetness impregnation of SiO_2 gel initially with aqueous $Mn(NO_3)_2$ at 90 °C, dried at 120 °C, with subsequent impregnation of aqueous $(NH_4)_5H_7(WO_4)_6$ and $M(NO_3)$ where M = Li, Na, K, Ba, Ca, Fe, Co, Ni, and Al; followed by calcination in air at 830−850 °C for 6 h	XRDL Cu K_α (ambient) Raman: 514.5 nm (ambient) XPS: Mg K_α (UHV)	XRD showed Na_2WO_4, $Na_2W_2O_7$, $MnWO_4$, and (α- cristobalite) Raman showed bands at 900−950 cm^{-1} in pre- and post-OCM catalysts, which the authors did not explain well
27	incipient-wetness impregnation of aqueous Na_2WO_4 onto amorphous SiO_2 support (Davisil-TM), dried at 120 °C for 8 h and calcined in air at 750−900 °C for 8 h	XRD: Cu K_α (ambient)	Na_2WO_4, SiO_2 (α-cristobalite)
23	Mn−W/SiO_2: incipient-wetness impregnation of aqueous $Mn(NO_3)_2$ and Na_2WO_4 onto SiO_2 (Aldrich Davisil 23,684−5) W/SiO_2: incipient-wetness impregnation of aqueous $(NH_4)_2WO_4$ onto SiO_2 Na/SiO_2: incipient-wetness impregnation of aqueous NaOH onto SiO_2, dried at 120 °C for 6 h and calcined in O_2 at 850 °C for 8 h, which transforms the amorphous silica to SiO_2 (α-cristobalite) W−Na/SiO_2: incipient-wetness impregnation of aqueous $(NH_4)_2WO_4$ onto precalcine Na/SiO_2.	XRD: Cu K_α (ambient) XPS: Mg K_α (UHV)	Na_2WO_4, Mn_2O_3, SiO_2 (α-cristobalite)

DOI: 10.1021/acscatal.9b01585
ACS Catal. 2019, 9, 5912−5928

Table 2. continued

ref	catalyst synthesis	characterization techniques	phases detected
	all above catalysts were dried for 6−8 h at 120 °C and calcined in oxygen at 850 °C for 8 h		
76	catalysts prepared by Li et al. and provided to Yoshida for analysis most likely by fluidized bed processing method[77]	XPS: Mg K_α and Al K_α (UHV at 620 °C) XANES: tungsten L_I edge, Mn K edge (ambient) EXAFS: tungsten L_{III} edge, Mn K edge (ambient)	amorphous MnO_6 and amorphous WO_4 phases on post-OCM catalyst
13	Mn−W−Na/SiO_2: slurries of aqueous $Mn(NO_3)_2$ and Na_2WO_4 with SiO_2 gel stirred at RT for 5 h and at 180 °C for 1 h; dried at 100 °C overnight and calcined in air at 550 °C for 2 h	XRD: Cu K_α (in situ).	XRD showed that Mn_2O_3 and Na_2WO_4 disappears under CH_4 reduction step at 800 °C
	Ti−Mn−W−Na/SiO_2: prepared by ball-milling of crystalline Mn_2O_3, TiO_2 and Na_2WO_4 crystalline powders with amorphous SiO_2 for 2 h	Raman: 532 nm (in situ at 800−720 °C) XPS: Al K_α (UHV)	Raman showed that $MnWO_4$ was formed under CH_4 reduction step at 800 °C, which changed to Mn_2O_3 under O_2 oxidation step at 760 °C
33	2%Mn−1.6%Na−3.1%W/SiO_2 was prepared by sequential incipient-wetness impregnation; the SiO_2 support (SiO_2 gel Davisil 646, ∼250−500 μm) was initially impregnated by an aqueous sodium tungstate dihydrate $Na_2WO_4{\cdot}2H_2O$ and $Na_2C_2O_4$ solution at 80 °C. The Na−W/SiO_2 was dried at 120 °C for 6 h and impregnated by an aqueous $Mn(CH_3COO)_2{\cdot}4H_2O$; catalysts dried at 120 °C for 6 h and calcined in air at 850 °C for 6 h with a heating rate of 2 °C/min	XRD-computed tomography at ESRF: (operando)	Mn_2O_3, SiO_2 (α-cristobalite), Na_2WO_4 phases disappeared at OCM conditions
78	SiO_2 support was impregnated with an aqueous solution containing appropriate concentration of $(CH_3COO)_2Mn{\cdot}4H_2O$ (Fluka, >99%) at room temperature; these materials were then dried in air at 75 °C overnight; after that the obtained materials were impregnated with an aqueous solution containing the appropriate concentration of $Na_2WO_4{\cdot}2H_2O$ (Sigma-Aldrich, min. 99%) at room temperature; samples were dried in air overnight at 75 °C; the calcination process was performed in air, heating the samples for 4 h from room temperature up to 750 °C (with a heating rate of approximately 3 °C/min) and holding the temperature for 1 h at 750 °C, consecutively	in situ XRD: Ni filtered Cu K_α radiation at 750 °C; the flow rate was 100 mL/min with the feed gas composition of CH_4:O_2:He = 4:1:4	SiO_2 (cristobalite, tridymite, quartz) and significant amounts of $MnWO_4$ phase formed under reaction; unlike the ex situ XRD, in situ XRD did not support presence of Na_2WO_4, $MnMn_6SiO_{12}$.

DOI: 10.1021/acscatal.9b01585
ACS Catal. 2019, 9, 5912−5928

however, shows that almost all major investigations of this catalyst system used the $Na_2WO_4{\cdot}2H_2O$ precursor as the source of both Na and W. In every report using this precursor, formation of only crystalline phases were readily detected with XRD and Raman spectroscopy. When *individual* oxide precursors of Na, Mn, and W were used (e.g., ammonium para-tungstate (APT), manganese nitrate, and sodium nitrate), broader and weaker bands *not* corresponding to any crystalline phases (e.g., $MnWO_4$, Na_2WO_4, WO_3, $Na_2W_2O_7$) at 910−950 cm^{-1} were also observed in the Raman spectra.[54] Given that Raman spectroscopy is sensitive to poorly ordered, dispersed metal oxide phases, it can be assumed that dispersed species were present along with crystalline phases on the SiO_2 support when individual precursors were employed in the synthesis procedure, even if the authors did not appreciate the fact.

For all the investigations that employed $Na_2WO_4{\cdot}2H_2O$ as the Na and W metal oxide source,[13,14,23,27,49,54−57] both Raman and XRD detected the presence of crystalline Na_2WO_4 nanoparticles. In only one study[13] that employed $Na_2WO_4{\cdot}2H_2O$, the crystalline Na_2WO_4 phase was not detected because the in situ Raman spectra were collected at temperatures above the melting point (~698 °C) of crystalline Na_2WO_4. Although not clearly mentioned, the broad Raman band ~930 cm^{-1} identified in this study could be due to the molten Na_2WO_4 phase. Other investigations, that used individual precursors for Na and W metal oxides,[23,26,54,58,59] the Raman bands of crystalline Na_2WO_4 were observed along with broader bands in the 910−950 cm^{-1} region, which might be from dispersed WO_x phase, but were not identified by the authors. Surprisingly, none of the literature studies addressed the presence and importance of the dispersed WO_x phase on SiO_2 and only focused on the presence and role of the crystalline Na_2WO_4 phases.

In the pioneering work that first attempted to elucidate the structure−property relationship of the supported $Mn/Na_2WO_4/SiO_2$ catalyst, both IWI and PM methods (summarized in Table 1) were used with the IWI synthesis resulting in a more stable catalyst.[61,62] In a subsequent study by the same group, IWI, MS, and SG synthesis methods were investigated. The SG catalyst exhibited uniform surface and bulk distribution of the active components, compared to the IWI catalyst. In the IWI catalyst, the active components were mainly surface enriched. However, as in the SG catalysts, MS catalysts also showed uniform distribution of the active components throughout bulk and the surface.

In another study, a comparison of the IWI, MS, and POSS synthesized catalysts was conducted.[49] The small crystal size of Mn_2O_3 (<20 nm) was observed in the case of the POSS catalyst, in contrast to the IWI and MS catalyst with 40 nm size of the corresponding crystals. The SG synthesis approach was examined in a different study and compared with the IWI catalysts.[60] Catalysts synthesized using the SG method resulted in a more homogeneous distribution of the active structures than IWI catalysts, determined by SEM-EDX, ICP, and BET comparison.

To enable large batch synthesis of the catalyst, the fluidized bed processing (FP) method has also been utilized to prepare this catalyst.[63,64] In this process, amorphous SiO_2 was coated with aqueous solutions of Na_2WO_4 and $Mn(NO_3)_2$ in a fluidized bed, followed by high temperature calcination that enabled the transformation of SiO_2 from an amorphous to a crystalline phase. The active phases were mostly found on the surface of the catalyst (SEM-EDX) and were reported to be stable under reaction conditions. A small amount of Na was found to have migrated into the SiO_2 support.

The majority of studies have utilized the aqueous IWI synthesis method that results in enrichment of the active component near the surface of the catalyst and prevents active metal components from transporting deep into the bulk silica. Different preparation methods, such as SC and FS, which circumvent surface enrichment of the active components, were utilized by different research groups. This synthesis approach involves a reaction mixture of the preheated precursors and fuels that self-ignites to yield metal oxide powders. The active metal oxides were claimed to be distributed homogeneously throughout the bulk silica support, instead of enriching the surface layer. No characterization study, however, was undertaken to understand the structure−performance relationship of the catalytic active phases formed using this preparation method. Similarly, the catalyst prepared using the FS method had uniformly distributed active metal oxides both throughout the bulk and the surface and exhibited higher surface area compared to the IWI catalysts. The FS synthesis method is a single step process in which the precursor solutions are exposed to a burning flame and the combustion products are then collected using a vacuum pump and the catalysts were used for OCM without further heat treatment (calcination).

In addition, the long-term stability studies of the SG, POSS, SC, and FS catalysts are missing in literature making IWI the most studied preparation method leading to a thermally stable catalyst. It should be noted that the catalysts prepared using different methods were characterized ex situ, ambient conditions, that are far from OCM reaction conditions. Moreover, in some cases, only the initial catalyst structures were investigated with the spent catalysts not being characterized. The reported data about the crystalline metal oxide phases and surface area may be not representative of the phases present under OCM reaction conditions.

The characterization techniques applied to investigate the supported $Mn/Na_2WO_4/SiO_2$ catalyst system and their findings are given in Table 2. A major limitation of the reported characterization studies of supported $Mn/Na_2WO_4/SiO_2$ catalysts is that they predominantly have been performed under ambient conditions, exposed to air at room temperature, before or after the OCM reaction at ~800−900 °C.[23,26,27,30,31,67,68] Surprisingly, only one in situ XRD and Raman characterization of the supported $Mn/Na_2WO_4/SiO_2$ catalyst has been reported to date and focused on the role of Ti-doping to trigger the low-temperature $MnTiO_3$ redox cycle.[13] Given the dramatic structural changes that can take place between ambient and the very high temperature OCM reaction conditions, such as transformation of the SiO_2 support (α- to β-cristoballite),[63,69−72] tungsten oxide phase changes (crystalline WO_3, monoclinic → triclinic → orthorhombic → tetragonal)[73] and Mn_xO_y (crystalline MnO_2→ Mn_2O_3→ Mn_3O_4→ MnO),[74] the reported findings may not be relevant to OCM and more operando and in situ studies are needed to be conducted to determine the nature of the catalyst components under OCM reaction conditions. Typically, the OCM studies have characterized the catalyst structures/phases with X-ray diffraction (XRD), Raman spectroscopy, XPS, XANES, EXAFS, and chemically probed the catalyst with H_2−TPR, CH_4−TPR, NH_3/CO_2−TPD-IR, TGA, and DSC. Besides Raman and XPS spectroscopic techniques, almost all other characterization studies typically employ practices that detect *bulk crystalline phases* and not *surface dispersed phases*.

DOI: 10.1021/acscatal.9b01585
ACS Catal. 2019, 9, 5912−5928

Thus, no information is currently available in the literature about the nature of the surface sites, especially under OCM reaction conditions, and the crystalline catalyst phases determined from ex situ XRD and Raman spectroscopic characterization studies provide little information about the actual catalyst structures present during OCM.

In spite of this severe limitation in the current state of understanding the supported OCM $Mn/Na_2WO_4/SiO_2$ catalyst system, the literature reports from ex situ studies will be distilled for analysis and contrasted with information based on modern in situ and operando characterization studies to highlight the need to study the OCM catalysts under relevant reaction conditions. A summary of major literature reports and the employed characterization techniques is provided in Table 2.

The in situ and operando characterization studies clearly demonstrate that the supported $Mn/NaWO_4/SiO_2$ catalyst system is highly dynamic and must be investigated under relevant OCM reaction conditions to fully understand the nature of each catalyst component. Furthermore, it is critical that information about surface WO_x, MnO_x, and NaO_x phases and sites be obtained under OCM reaction conditions since they *must* play an important role in the OCM catalytic reaction.

Some of the highlights about OCM catalysts from Table 2 are as follows:

- With rare exceptions, the characterization studies were performed under ambient conditions (air exposed at room temperature) that are very far from the extreme OCM reaction conditions (>750 °C).
- Only crystalline phases were monitored with XRD and Raman spectroscopy.
- In the presence of Na, the initial amorphous SiO_2 phase crystallizes to SiO_2 (cristobalite).
- The operando and in situ characterization studies under OCM reaction conditions (>750 °C), however, demonstrates that most of the crystalline phases detected at room temperature are not present under OCM reaction conditions: SiO_2 (α-cristobalite → β-cristobalite), Na_2WO_4 → amorphous, $Na_2W_2O_7$ → not detected, Mn_2O_3 → negligible signal intensity, and $MnWO_4$ → might form under reaction conditions.
- Another in situ characterization study under oxidizing (O_2) and reducing (CH_4) environments at 900 °C revealed that Mn was present as Mn_2O_3 and $MnWO_4$, respectively, further revealing the dynamics of the crystalline phases with environmental conditions.
- The presence of W^{5+} was detected with XPS under UHV, but these are reducing conditions. EPR also detected W^{5+} under ambient conditions.
- Several Raman studies also detected broad, weak bands at ~910−950 cm^{-1}, which may arise from dispersed WO_x surface phase, but these band were either ignored or not assigned incorrectly to crystalline Na_2WO_4.

3. ACTIVITY OF OCM CATALYSTS

The catalytic OCM activity and selectivity of SiO_2-supported Na, Mn, and W catalysts indicates the presence of synergistic interactions between the catalyst components as shown in Figure 1.

Catalysts containing only Mn-oxide are active toward OCM but lack selectivity. Catalysts containing only W-oxide are both

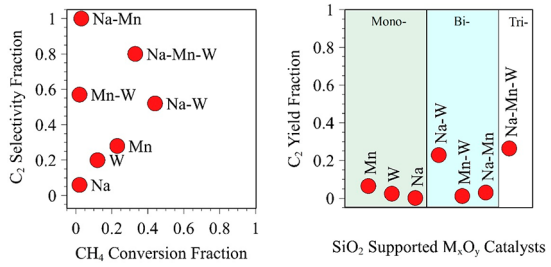

Figure 1. Synergistic influence of SiO_2 supported metal oxides toward CH_4 conversion and C_2 selectivity (left) and C_2 yield (right) for catalytic OCM reaction. Data adapted from refs 23, 27, and 58. Nominal weight loadings were chosen to mimic ~2% Mn_2O_3, 4−5% Na_2WO_4 catalyst. Na: (1123 K; GHSV = 2000 h^{-1}, CH_4:O_2 = 4.5; 0.4 g catalyst).[27] Na−Mn: (1073 K; CH_4:O_2 = 3:1; GHSV = 36 000 h^{-1}; 0.1 g catalyst).[58] W, Mn, Na−W, Mn−W, Mn−Na−W: (1123 K; CH_4:O_2 = 4.5:1; total flow rate = 18 cc/min; 0.4 g catalyst).[23]

inactive and unselective. The addition of Na to W-oxide catalysts increases their activity (most active toward OCM) and also leads to a dramatic increase in C_2 selectivity. The synergy of the Na−W-oxide system may be related to structural effects and introduction of basic surface sites. The addition of Na also makes tungsten oxide component easier to reduce that may have a positive implication for OCM.[66,79] The catalysts containing both Mn-oxide and W-oxide exhibited better selectivity but were slightly less active than the catalysts comprising of Mn-oxide alone. Interestingly, the Na−Mn-oxide system was 100% selective, but lacked any significant activity. The three component SiO_2 supported Mn−Na−W-oxide catalyst is slightly less activity than the most active Na−W-oxide catalyst but exhibits significantly higher selectivity. The role of each oxide for catalytic OCM is hard to ascertain since their structures under reaction conditions are still not known.[23]

The Na component has been shown to transform the SiO_2 support from its initial amorphous phase to the crystalline SiO_2 (α-cristobalite) phase.[63,69−72] It was initially proposed that the crystalline SiO_2 (α-cristobalite) phase plays a key role in the OCM reaction, but subsequent in situ characterization studies revealed that the SiO_2 (α-cristobalite) phase is actually not present under OCM reaction conditions as shown in Table 1. It was also argued that the phase transformation changes the amorphous SiO_2 support that is an efficient CH_4 combustion catalyst into the crystalline SiO_2 (α-cristobalite) phase that is an inert support.

4. PROPOSED ACTIVE SITES

The IWI synthesized catalysts have been most extensively investigated in the literature and, thus, only the proposed active sites for IWI prepared catalysts will be reviewed since other synthesis techniques lack characterization data or are rare. It is not straightforward to establish the nature of the active sites during OCM by the supported $Mn/Na_2WO_4/SiO_2$ catalysts because the reported characterization studies have almost completely been performed under ambient conditions that are quite far from OCM reaction conditions (see Table 1 and 2). Only a few in situ/operando studies have been reported for the supported $Mn/Na_2WO_4/SiO_2$ catalyst system and have focused on the bulk crystalline phases present during OCM.[13,33,78] Primarily SiO_2 (cristobalite) is detected since the other phases (Na_2WO_4, Mn_2O_3, etc.) are present in either molten or reduced states because of the high OCM reaction temperatures. The nature of the catalytic active sites on the

DOI: 10.1021/acscatal.9b01585
ACS Catal. 2019, 9, 5912−5928

Table 3. Summary of Proposed Roles of Na-, Mn-, and W-Oxide for OCM by Supported $Mn/Na_2WO_4/SiO_2$ Catalysts

ref	proposed role of Na	proposed role of Mn	proposed role of W
14	Na−O−Mn is active site	surface Mn site responsible for activation of molecular O_2	W thermally stabilizes the catalyst
	Na prevents complete oxidation of CH_4 by isolating Mn ions		
58	Na helps transport Mn to surface	CH_4 conversion and C_2 selectivity are closely related to surface Mn sites	Na−O−W bond is part of active site
	Na−O−Mn is part of an active site		
	catalyst surface is mostly Na and O		
26	addition of Na to WO_3/SiO_2 transformed WO_6 to WO_4 responsible for enhanced selectivity		distorted WO_4 responsible for C_2 product formation
			W−O bond order may correlate with C_2 selectivity
			shortest bond in WO_4 may be responsible for converting CH_4 to C_2 but does not attack C_2 as readily
30	Na transports Mn to surface	surface Mn activates gas phase molecular O_2	WO_4 and W−O−Si bonds are part of active site
	Na distorts WO_4, making the site selective toward C_2 products	pulse experiments in absence of O_2 still showed reduction of Mn^{3+} to Mn^{2+}	CH_4 pulse experiments showed reduction of W^{6+} to W^{5+}
			EPR data and references of W^{5+} used to argue about presence of W^{4+}
56	Na helps transform amorphous silica to crystalline SiO_2 (α-cristobalite)	Mn present as Mn_2O_3 crystallites	W═O and 3 W−O restructured cluster is proposed to be an integral part of the OCM active site
57		lattice O^{2-} is involved in OCM	
		F centers formed on WO_4 (i.e., crystallographic defect in which an anionic vacancy in crystal is filled by one or more unpaired electrons) activate gas phase molecular O_2 to lattice oxygen. Mn increases mobility of surface lattice oxygen	
54	transforms amorphous silica to crystalline SiO_2 (α-cristobalite)		
27	Na promotes transformation of amorphous silica to SiO_2 (α-cristobalite)		W switches on OCM activity. Alkali stabilized, W═O bond is the active site
	Na is both a structural and chemical promoter		
23	Na promotes transformation of amorphous silica to crystalline SiO_2 (α-cristobalite) that is responsible for selectivity of C_2 products		most likely WO_4 is part of active site
	Na disperses WO_4 on the surface of the SiO_2 support		
76		MnO_4 and surface unsaturated MnO_6 sites detected after OCM reaction	surface has WO_4 sites, but after 450 h OCM operation none detected
		combination of MnO_4 and MnO_6 sites in different oxidation states responsible for OCM	
13		$Mn^{3+} \leftrightarrow Mn^{2+}$ redox cycle involved in molecular O_2 activation; TiO_x doping accelerates OCM reaction	redox mechanism for W involves a 2 electron process: $W^{6+} \rightarrow W^{4+}$ and $W^{4+} \rightarrow W^{6+}$
		XRD and Raman show that Mn_2O_3 and $MnWO_4$ are formed.	broad and weak Raman band at 930−1000 cm^{-1} from possible dispersed WO_x phase not addressed

DOI: 10.1021/acscatal.9b01585
ACS Catal. 2019, 9, 5912−5928

catalyst surface during OCM is still unknown (e.g., possible presence of dispersed surface metal oxide sites on the SiO_2 support and the surface composition of the 3D oxide phases (molten and crystalline)). It should be emphasized that heterogeneous catalysis is a surface phenomenon and bulk structural information does not provide information about the surface active sites. Even though the actual structures of the surface catalytic active sites under OCM reaction conditions are still not known, this has not stopped researchers from proposing structure−activity relationships in the literature. Interestingly, most of such speculations were not supported by the experimental data provided by the authors in the original papers, and in fact some of the data contradicts the authors' speculations. For example, the active site was proposed to contain W^{4+}, but in cited publications and in the data provided in the report, W^{5+} can be observed.[30,80] Nonetheless, the speculative models proposed for the active sites and the roles of each catalyst component is summarized in Table 3.

The information in Table 3 shows that almost all possible types of active sites for OCM have been proposed in the literature without solid experimental proofs, reflecting the creative imagination of the OCM researchers. These studies have also assigned a large set of roles to the active metal oxides toward catalyst structure, active site and catalytic OCM reaction performance. A summary of the roles is presented next. Although Na is known to accelerate the crystallization of the amorphous SiO_2 support, Na has also been proposed to (i) disperse WO_4 on SiO_2, (ii) distort WO_4 making it selective toward C_2 products, (iv) transform WO_6 to WO_4 that are more selective, (v) form Na−O−Mn bond that is the active site, (vi) surface segregate Mn, and (vii) prevent complete oxidation of CH_4 by isolating Mn ions. The most common role proposed for Mn is its association with the catalyst redox properties, such as (i) surface Mn activates gas phase molecular O_2, (ii) Mn increases mobility of surface and bulk lattice oxygen, (iii) $Mn^{3+} \leftrightarrow Mn^{2+}$ redox cycle involved in OCM, (iv) combination of MnO_4 and MnO_6 in different oxidation states are active sites for OCM, and (v) surface MnO_x sites responsible for OCM activity and C_2 hydrocarbon selectivity. Similarly, W has been proposed to (i) impart thermal stability to the catalyst, (ii) surface WO_4 is the active site for OCM involving its W═O and W−O−Si bonds, (iii) WO_4 responsible for C_2 hydrocarbon selectivity, (iv) undergo $W^{6+} \leftrightarrow W^{4+}$ redox cycle, and (iv) undergo $W^{6+} \leftrightarrow W^{5+}$ redox cycle. The OCM literature has been adamant throughout the years about the presence of surface tungsten oxide sites on SiO_2 as being present as WO_4 sites even though their characterization studies only detect the presence of crystalline Na_2WO_4, $MnWO_4$, and WO_3 phases. Unfortunately, all of these proposals do not have supporting information in the absence of detailed surface information, especially under OCM reaction conditions, and are, thus, highly speculative.

The nature of the dispersed tungsten oxide phase on SiO_2 has been extensively investigated, but the OCM literature seems to ignore these relevant studies.[32,81−83] The SiO_2-supported tungsten oxide phase contains both a dispersed surface phase (986 cm^{-1}) and crystalline WO_3 nanoparticles (810, 707, and 215 cm^{-1}) with the distribution between the two phases deepening on tungsten oxide loading and synthesis method. The dispersed surface tungsten oxide phase consists of isolated surface dioxo WO_4, $(O═)_2W(−O−Si)_2$, sites under dehydrated conditions.[32,81−83] SiO_2-supported tungsten oxide clusters (polyoxometallates (POMS) of Keggins ($[W_{12}O_{40}]^{3−}$) and Dawson ($[W_{18}O_{62}]^{6−}$)) were also investigated and shown not to be presented because of their thermal decomposition to the isolated surface dioxo WO_4 sites at elevated temperatures.[81] In light of this information, the weak and broad Raman bands detected in the 910−950 cm^{-1} region for the supported $Mn/Na_2WO_4/SiO_2$ catalysts under ambient conditions may very well be associated with surface tungsten oxide phases, but the nature of this surface tungsten oxide phase was not addressed and completely ignored. Future studies must address the nature of such a surface tungsten oxide phase and determine if it represents the catalytic active site for the OCM reaction.

5. REACTION KINETICS, REACTION PATHWAYS, AND RATE-DETERMINING-STEP

One distinctive feature of OCM is that it follows a heterogeneous−homogeneous (heterohomo) reaction pathway where CH_4 activation takes place on the catalyst active sites to produce gaseous methyl radicals, CH_3•, (heterogeneous step) that subsequently couple in the gas phase to form C_2H_6 (homogeneous step). This heterohomo reaction pathway complicates the analysis of experimental catalytic OCM data since separation of the gas-phase reactions from the surface reactions is not straightforward. In addition to the selective C_2H_6/C_2H_4 reaction pathways, the hydrocarbon molecules (CH_4, C_2H_4, and C_2H_6) also undergo overoxidation to carbon oxides (CO and CO_2) that may take place both in gas-phase and on the surface of the catalyst. These multiple heterohomo reaction pathways have limited the current understanding of the catalytic OCM kinetics. Several reviews discussing the general kinetic behavior of a large set of OCM catalysts are available in the literature.[8,9] However, the catalytic OCM reaction pathways are dependent on the type of the catalyst under investigation. In contrast, a concise, yet thorough review of catalytic OCM reaction kinetics on the supported $Mn/Na_2WO_4/SiO_2$ catalyst is presented here by critically analyzing the rationality of kinetic parameters, individual reaction pathways, rate-determining-step, most abundant reaction intermediate and overall reaction kinetics.

To obtain kinetic data and reaction mechanism information, experiments with cofeeding and in pulse mode have been extensively conducted.[84] Differential reaction conditions were implemented to minimize the effect of hot spots from the exothermic OCM reaction in the reactor. The overall catalytic OCM reaction was found to be first-order in the partial pressure of CH_4 and 1/2-order in the partial pressure of oxygen.[85,86] These kinetic reaction orders reflect the adsorption of CH_4 on the catalyst surface and the dissociative adsorption of gas phase molecular O_2 to surface O* species on the catalyst. The overall activation energy for the catalytic OCM reaction was found to be ∼268 kJ/mol for the supported $Mn/Na_2WO_4/SiO_2$ catalysts.[84] Isotope-labeling experiments were employed to examine the kinetics of activation of the methane C−H bond and the O−O bond of molecular O_2.[85] A kinetic isotope effect (KIE) of ∼1.24−1.29 was found for $CH_4−O_2$ versus CD_4-O_2 for a range of O_2 partial pressure (0.9−3.5 kPa) showing that breaking the C−H/C−D bond of methane is involved in the rate-determining-step. Experiments with the $CH_4−CD_4−O_2$ isotope reactant mixture produced negligible amounts of the mixed isotope $CH_{4−x}D_x$ product reflecting the irreversibility of the C−H bond-breaking activation step and the efficient conversion of H/D to water. Further investigation with the $CH_4−{}^{18}O_2−{}^{16}O_2$ oxygen isotope

DOI: 10.1021/acscatal.9b01585
ACS Catal. 2019, 9, 5912−5928

reactants found evidence for formation of mixed $^{16}O^{18}O$ isotope product that decreased with increasing CH_4 conversion. These observations suggest that the gas phase molecular O_2 dissociatively adsorbs on the catalyst surface in a reversible manner. Temporal analysis of products (TAP) reactor studies, which operates in the Knudsen diffusion regime with negligible gas phase collisions, demonstrated that coupling of CH_3• radicals takes place in the gas-phase since small pulses of CH_4 (10^{17} molecules) do not form C_2 products.[87] Gas-phase coupling of methyl radicals was also concluded from matrix isolation electron spin resonance (MI-ESR) and resonance enhanced multiphoton ionization (REMPI) measurements with transition metal oxides ($LiNiO_2$ and $NaMnO_4/MgO$, experimental temperature = 650−900 °C) showed that CH_4 and surface O* react to form surface CH_3• radicals that desorb and dimerize to form C_2H_6 in the gas phase.[88−90]

To understand the origin of C_2H_4 (directly from CH_4 or indirectly from C_2H_6), a series of experiments using $CH_4 + O_2$ and $C_2H_6 + O_2$ were conducted under differential and integral reaction conditions.[84] At very low conversion of CH_4 (differential reaction conditions), only a small amount of C_2H_4 is formed via a direct route from CH_4. On the other hand, at high conversion of CH_4 (integral reaction conditions), the majority of the ethylene is produced from C_2H_6. Furthermore, C_2H_4 selectivity was found to sharply decrease (with a drastic change in slope) at very low conversion of CH_4 (<1%) (for a range of oxygen partial pressures) while the C_2H_6 formation rate decreased in a linear manner.[85] These studies reveal that C_2H_6 is a primary reaction product from CH_4−O_2 and C_2H_4 is a secondary reaction product formed from dehydrogenation of C_2H_6 (via both oxidative-surface catalyzed and thermal gas-phase reactions).

The formation of CO and CO_2 follow both primary and secondary reaction pathways as they are also formed by over oxidation of hydrocarbons (CH_4, C_2H_6, and C_2H_4).[85,86] The CH_3• radicals, which couple to form C_2H_6, may also undergo over oxidation to form CO and CO_2.[88] At very low conversion of CH_4, the formation rate of CO showed a stronger dependence on molecular O_2 partial pressure than that of the CO_2 formation rate over a range of O_2 partial pressure (1−15 kPa).[85] This trend assumes that reaction of CH_3• radical with gas phase O_2 ($\sim P_{O_2}$) results in formation of CO and that CO_2 formation takes places via reaction of CH_3• radical with surface O* ($\sim P_{O_2}^{0.5}$). The sticking coefficient of CH_3• radicals on oxide catalysts (ZnO, CeO_2, La_2O_3, Sr/La_2O_3, and Li/MgO at 650 °C) has been determined by the ratio of number of CH_3• reacted on a metal oxide to the number of collisions between the CH_3• and the metal oxides and was found to be very low (highest value is $\sim 10^{-5}$ for ZnO catalyst[91]). From this finding, it can be inferred that the sticking coefficient of methyl radical on Mn_2O_3−Na_2WO_4/SiO_2 catalyst at high temperature (>800 °C) will be very low and the reaction of CH_3• radical with surface O* after desorption will be extremely difficult.[84] Such a low sticking probability for adsorption of methyl radicals on the catalyst proves the experimental finding that at low O_2 partial pressure, the C_2 product selectivity is increased, even if the catalyst surface remains in the oxidized state. For low C_2H_6 conversion, the oxidation of C_2H_6 was found to correlate with partial pressure of C_2H_6 and showed almost no dependence on partial pressure of oxygen.[92] This suggests that C_2H_6 oxidation to C_2H_4, CO and CO_2 mostly proceeds via surface reactions. Isotopic-labeling experiments with $^{12}CH_4$ and $^{13}C_2H_4$ found that the formation of carbon oxides from ethylene is ∼6−8 times faster than from complete oxidation of CH_4,[84] which is in qualitative agreement with other investigations that found that combustion of C_2H_4 to be ∼4.3 times faster than CH_4 combustion.[85] To understand the overoxidation of C_2H_4, experiments with and without supported $Mn/Na_2WO_4/SiO_2$ catalyst were conducted. It was claimed that the undesired overoxidation of C_2H_4 to CO_x proceeds via both surface and gas-phase reactions with the rate constant of the surface reaction about 4 times faster than the gaseous reaction at 800 °C.[84] Interestingly, the presence of gas-phase CH_4 was found to reduce C_2H_4 overoxidation.[84] This behavior was also observed in another investigation, which suggests that under normal catalytic OCM reaction conditions, reactant CH_4 competes with the C_2 products for surface phase reaction.[86] Oxidation of C_2H_4 on the catalyst surface, for low C_2H_4 conversion, was investigated in a different study.[92] For deep oxidation of C_2H_4, the activation energy for formation of CO (∼75 kJ/mol) was found to be significantly higher than the activation for formation of CO_2 (∼40 kJ/mol), which is consistent with the greater CO generation with increasing temperature of the catalytic OCM reaction.

The relative ratio of gas-phase vs catalytic surface reactions has been examined by independently flowing the reaction mixture into an empty reactor and a reactor filled with the supported $Mn/Na_2WO_4/SiO_2$ catalyst.[86] The heterogeneous surface catalytic reaction contribution was determined by subtracting the homogeneous gas-phase reaction data for the empty reactor from the data for the reactor filled with catalyst. Information from these experiments are reliable as long as the residence time of the reactant gases for empty versus catalyst filled reactor and effects of gas-phase reactions on surface reaction network are neglected. For low partial pressure of molecular O_2 (<10 kPa), the oxygen conversion predominantly proceeds through surface phase reaction, that is oxygen is dissociatively activated on the catalyst surface resulting in reoxidation of metal oxides. Above 10 kPa O_2 partial pressure, the gas phase O_2 conversion was found to significantly increase with O_2 partial pressure. This is expected because reoxidation of the catalyst surface is a very fast process (∼100 times faster) than its reduction by CH_4.[92] The individual contribution of gas-phase vs. catalytic surface phase CH_4 conversion and formation of C_2H_6 and H_2O was found in accordance with the O_2 conversion data (predominantly surface phase below 10 kPa and increasingly higher gas-phase reaction contribution above 10 kPa of oxygen partial pressure).[86] Interestingly, CO and CO_2 were found to form through gas-phase and catalytic surface phase reactions, respectively, for O_2 partial pressure in the range of 1−30 kPa.[86] This behavior was also observed in a previous study (discussed above).[85] As expected, all the H_2 was formed in the gas phase due to thermal dehydrogenation of C_2H_6 since only thermal dehydrogenation process will form H_2 and surface mediated reaction will form H_2O because of the high surface concentration of O*.

Kinetic modeling of catalytic OCM reaction rates has been undertaken to interpret the observed experimental reaction rates and to provide kinetic models with predictive capabilities for optimization of the reaction conditions. As indicated above, the simultaneous presence of heterohomo reactions during catalytic OCM complicates determining the contributions from surface and gas-phase reactions, respectively. An extended model for the gas phase reactions has been proposed that

DOI: 10.1021/acscatal.9b01585
ACS Catal. 2019, 9, 5912−5928

Table 4. Rate Expressions and Kinetic Parameters for the Catalytic OCM Reaction by the Supported $Mn/Na_2WO_4/SiO_2$ Catalyst

	reaction order		activation energy (kJ/mol)			
reference	CH_4 (m)	O_2 (n)	CH_4	C_2H_6	rate expression (CH_4 activation reaction)	reaction mechanism of catalytic CH_4 activation
85	1	0.5	290[b]		$^*R_{CH_4}\alpha k P_{CH_4} P_{O_2}{}^{0.5}$[a]	power law
16	1	0.75	213	153	$\dfrac{k P_{CH_4}{}^m P_{O_2}{}^n}{(1 + K_{CH_4}P_{CH_4} + K_{O_2}P_{O_2})^2}$	Langmuir–Hinshelwood (L–H)
99	0.5	0.5	133	230		
100			149	263	$R_{CH_4}\alpha k\theta_O P_{CH_4}$	Eley–Rideal (E–R)
101			148	134		
92	1	1	192	180	$R_{CH_4}\alpha \dfrac{k_{red}P_{CH_4}k_{ox}P_{O_2}}{k_{red}P_{CH_4} + k_{ox}P_{O_2}}$	Mars–van Krevelen (MvK)
97			275			

[a]For low surface O* coverage and [b]anhydrous condition.

consists of 1582 reaction steps, but the practical implementation of this network is limited due to the large set of data that can overwhelm the data handling and manipulation.[93] The gas-phase reaction network, however, has been considered to be very well described by this model.[94] A smaller model for the gas-phase reactions containing only 39 elementary reaction steps has also been developed.[95,96] Both of these models only account for the gas-phase homogeneous reactions, making them valid for any catalyst system, but they do not address the surface catalyzed reactions. Kinetic models for heterogeneously catalyzed surface reactions have also been developed.[87,97] In these models a dissociative adsorption of the gas phase O_2 on the catalyst surface was reported, which is responsible for the activation of CH_4 molecule.

Formal models composed of both gas-phase and surface catalyzed reactions are common in the literature and effectively account for the overall OCM kinetics.[16,92,98−101] Comparison of the kinetic parameters (activation energy for CH_4 and C_2H_6 activation, reaction orders, rate expressions and proposed mechanisms) and the elementary steps of the catalytic OCM reaction networks proposed by the above models are presented in Tables 4 and 5, respectively. Many discrepancies exist in the literature regarding the measurements of kinetic parameters, as well as defining and validating elementary reaction steps for the catalytic OCM reaction.

The critical kinetic observations, differences and conclusions from these models are discussed next. The power law dependence of the rate of CH_4 oxidation on the partial pressure of CH_4 and molecular O_2 were measured and a formal power-law model was suggested by different groups.[84−86] In a different study, the CH_4 conversion (at 850 °C, $CH_4/O_2 = 5$) was found to level off at a space time of 30 kg·s/m^3.[16] The authors further commented that gas phase O_2 is required for CH_4 oxidation and a nonoxidative route is not present for this reaction. However, it must be noted that this observation is not unique in the sense that the CH_4 conversion will always reach a steady-state value due to the complete conversion of oxygen at high CH_4 to oxygen ratio ($CH_4/O_2 = 5$). Another investigation found CH_4 conversion to increase slightly with increasing partial pressure of O_2[99] that could be due to the increased contribution of the gas-phase reaction at high O_2 partial pressure.[86] On the basis of these analyses, the Langmuir–Hinshelwood type mechanism (see Table 4)—as proposed by these researchers—could only be an artifact of experimental conditions imposed in the corresponding studies. Moreover, both of these studies did not consider the dissociative adsorption of gas-phase molecular O_2 on the catalyst surface[85] that introduces an intrinsic fundamental error in to the defined models.

New models with dissociative O_2 adsorption were developed to address the absence of dissociative adsorption of gas-phase molecular O_2.[98,100,101] Some of these models, however, are not reliable because they failed in explaining the rate-determining-step[98] and contain a relatively large error (>20%) between the model parameters and experimentally determined values.[100] An alternative microkinetic model was derived with 39 gas-phase and 11 surface catalyzed elementary reaction steps. Model optimization through sensitivity analysis and determination of the sticking coefficient, predicted that surface vacant sites and surface O* species significantly cover the catalyst surface during OCM. On the basis of this observation, surface O* sites were considered as the most abundant reaction intermediate (MARI) and an Eley–Rideal (E–R) type mechanism was proposed for CH_4 oxidation.[101] Both Langmuir–Hinshelwood and Eley–Rideal type mechanism consider the occurrence of adsorption–desorption equilibrium with respect to all reactants (or at least one for E–R), which is practically impossible at typical catalytic OCM reaction temperatures (750–900 °C) because of their low heat of adsorption.[9] Alternatively, a few studies found experimental evidence (production of C_2H_6, CO, and CO_2) for oxidative CH_4 reaction in the absence of gas-phase O_2, which suggests a Mars–van Krevelen (MvK)-type mechanism where the oxidation reactions proceed through the involvement of lattice oxygen from the catalysts.[92,97] The evidence for the MvK-type mechanism can be found in other studies as well.[87,97] In pulse experiments, no quantitative change in C_2H_6 formation was observed with increase in delay time for with O_2 pulses after the initial CH_4 pulse.[87] This reveals that the quantitative CH_4 oxidation to C_2H_6 does not depend on gas-phase O_2 concentration as long as sufficient reactive lattice oxygen is available in the catalyst. This is supported by TAP reactor studies in the absence of gas- phase reactions, where an isotope switch from $CH_4-{}^{16}O_2 \rightarrow CH_4-{}^{18}O_2$ demonstrated that ^{18}O-containing products were only observed after a large volumetric input of CH_4-$^{18}O_2$ suggesting involvement of large amounts of catalyst lattice oxygen during the OCM reaction. On the basis of the above experimental arguments, the MvK mechanism seems most relevant for the OCM reaction by the supported $Mn/Na_2WO_4/SiO_2$ catalysts.

No consensus regarding the catalytic OCM reaction pathways is found in the catalysis literature (see Table 5). A

DOI: 10.1021/acscatal.9b01585
ACS Catal. 2019, 9, 5912−5928

Table 5. Reaction Network As Suggested/Modeled by Different Groups

	reaction network/reference	100	101[a]	92	87	97
	adsorption/desorption					
R1	$O_2 + s \leftrightarrow O_2(s)$				•	•
R2	$O_2(s) \leftrightarrow yO_x(s)$				•	
R3	$O_2(s) \leftrightarrow O_{elec}(s) + O_{nulc}(s)$					•
R4	$O_2 + 2s \leftrightarrow 2O(s)$	•	•			
R5	$2OH(s) \leftrightarrow H_2O + O(s) + s$	•	•		•	
R6	$4OH(s) + O_2 \leftrightarrow 2H_2O + 4O(s)$			•		
R7	$H_2O(s) \leftrightarrow H_2O + s$					
	catalytic surface reactions					
S1	$CH_4 + O(s) \rightarrow CH_3\bullet + OH(s)$	•	•	•	•	
S2	$CH_4 + O_{elec}(s) \rightarrow CH_3\bullet + OH(s)$					•
S3	$CH_4 + O_{nulc}(s) \rightarrow CO_x$			•		•
S4	$C_2H_6 + O(s) \rightarrow C_2H_5\bullet + OH(s)$	•	•	•	•	•
S5	$C_2H_5\bullet + O(s) \rightarrow C_2H_4 + OH(s)$	•		•		•
S6	$CH_3^\bullet + O(s) \rightarrow CH_3O(s)$		•			
S7	$CH_3O(s) + O(s) \rightarrow CH_2O(s) + OH(s)$		•			
S8	$CH_2O(s) + O(s) \rightarrow HCO(s) + OH(s)$		•			
S9	$CH_3^\bullet + 3O(s) \rightarrow CHO(s) + 2OH(s)$	•				
S10	$CHO(s) + O(s) \rightarrow CO(s) + OH(s)$		•			
S11	$CHO(s) + O(s) \rightarrow CO + OH(s) + s$	•				
S12	$CO(s) + O(s) \rightarrow CO_2(s) + s$					
S13	$CO(s) + O(s) \rightarrow CO_2 + 2s$		•			
S14	$CO + s \rightarrow CO(s)$		•			
S15	$CO_2 + s \rightarrow CO_2(s)$					
S16	$CO + O(s) \rightarrow CO_2 + s$	•				
S17	$C_2H_4 + O(s) \rightarrow C_2H_4O(s)$					
S18	$C_2H_4(s) + O(s) \rightarrow C_2H_3(s) + OH(s)$					
S19	$C_2H_4 + O(s) \rightarrow C_2H_3^\bullet + OH(s)$	•			•	
S20	$C_2H_3(s) + OH(s) \rightarrow CH_2O(s) + HCO(s)$					
S21	$4HO_2^\bullet \rightarrow 3O_2 + 2H_2O$					
S22	$xO_2(s) + CH_4 \leftrightarrow CO_y + zH_2O(s)$				•	•
S23	$xO_2(s) + C_2H_6 \leftrightarrow 2CO_y + zH_2O(s)$				•	
S24	$xO_2(s) + C_2H_4 \leftrightarrow 2CO_y + zH_2O(s)$				•	•
	gas-phase reactions					
G1	$2CH_3^\bullet \rightarrow C_2H_6$	•		•	•	•
G2	$CH_3^\bullet + O_2 \rightarrow CHO^\bullet + H_2O$	•				
G3	$CH_3^\bullet + O_2 \leftrightarrow CH_3O_2$			•		
G4	$CH_3^\bullet + CH_3O_2 \rightarrow CO_x$			•		
G5	$CH_3O_2 + CH_3O_2 \rightarrow CO_x$			•		
G6	$C_2H_3^\bullet + O_2 + OH^\bullet \rightarrow 2CHO^\bullet + H_2O$	•				
G7	$CHO^\bullet + O_2 \rightarrow CO + HO_2^\bullet$	•				
G8	$CO + HO_2^\bullet \rightarrow CO_2 + OH^\bullet$	•				
G9	$C_2H_6 \rightarrow C_2H_5^\bullet + H^\bullet$	•				•
G10	$C_2H_5^\bullet \rightarrow C_2H_4 + H_2$	•				•

[a]The 39 gas phase reactions are not included in the table and can be found in the corresponding references.

DOI: 10.1021/acscatal.9b01585
ACS Catal. 2019, 9, 5912−5928

major difference observed for adsorption−desorption of the elementary steps as proposed by different models is the activation of gas-phase molecular O_2 on the catalyst surface (see Table 4). The majority of the models proposed dissociative adsorption of O_2 via (i) activation of gas phase O_2 at two vacant adjacent surface sites,[100,101] (ii) adsorption of gas phase O_2 on an active surface site with a fraction dissociating to form surface atomic oxygen,[87] and (iii) adsorption of gas-phase O_2 on an active site that subsequently dissociates to two different types of surface atomic oxygen (electrophilic and nucleophilic).[97] In the last two cases, the adsorbed molecular O_2 and the nucleophilic atomic oxygen, respectively, are nonselective (cause overoxidation to carbon oxides), whereas the dissociated and electrophilic oxygen atoms are responsible for C_2H_6 production.

Another model considered that the lattice oxygen atoms are strongly bound to the catalyst lattice.[92] The authors proposed that reoxidation of the catalyst takes place via an oxidative dehydrogenation mechanism, without intermediate dehydroxylation (see **R5** and **R6** in Table 5). At the high temperature of the catalytic OCM reaction, however, the lattice oxygen atoms are not very strongly bound as desorption of oxygen (starting at 725 °C) into the gas phase was observed during temperature-programmed desorption (O_2-TPD).[97] Currently, most of the researchers on OCM agree that the selective oxygen species involved in the rate-determining-step of the OCM reaction are the lattice oxygen from the catalyst (MvK mechanism) and not the reactant gas-phase molecular O_2 reactant (L−H or E−R mechanisms).[102]

For the surface reactions, the major difference was the exclusion of the oxidation step of ethyl radical on the catalyst surface to form ethylene (see S5 in Table 5).[87,101] This conclusion was made on the basis of sensitivity analysis that excludes the importance of this reaction.[101] The determination of sticking coefficient (in the microkinetic model with first approximation value of 0.2) of ethyl radical ($\sim 10^{-7}$; ~100 times smaller than sticking coefficient of methyl radical) on the catalyst surface suggests that there is limited possibility of occurrence of this reaction. Additionally, depending on O_2 activation on the catalyst surface, gas-phase CH_4 can directly react with nonselective (nucleophilic) oxygen to form deep oxidation products (carbon oxides).[97] This is substantiated by another model, which experimentally found that at constant CH_4 partial pressure, the heterogeneous deep oxidation of CH_4 to carbon oxides is first-order in the partial pressure of O_2 (in contrast to 1/2-order for C_2H_6 formation).[92] Looking at the gas-phase elementary reactions in Table 2, only one model considered the oxidation of methyl radical with molecular O_2 to form the CH_3O_2· molecule (reactions **G3**, **G4**, and **G5** in Table 5).[92] In contrast, in a catalytic reactor at very high temperatures, the thermodynamic equilibrium strongly favors formation of CH_3· and O_2 compounds rather than the CH_3O_2· radical.[103]

5.1. Effect of Pressure. Industrial application of any process requires high operating pressure conditions to make the processes economically viable (smaller reactor size, effective product separation, reduced energy input), but detail studies of the catalytic OCM reaction at high pressures are very limited in the literature. With an increase in pressure, the production of C_2H_6 and C_2H_4 increases, up to a maximum pressure, after which the gas phase reaction becomes dominant (which can be suppressed by operating the reactor at high space velocity).[87,104] This suggests that an optimum operating pressure value exists for maximum C_2H_6/C_2H_4 production; however, such a pressure limit is yet to be determined for the supported Mn_2O_3−Na_2WO_4/SiO_2 catalyst.[87] A few other studies examined the supported Mn_2O_3−Na_2WO_4/SiO_2 catalyst performance (at high pressure and low gas space velocities) and found it to be sufficiently active even at a notably lower temperature (~25% C_2 yield at 735 °C in contrast to same C_2 yield at 800 °C for atmospheric operating pressure.)[105,106]

5.2. Effect of H_2O. Addition of H_2O was found to result in higher OCM rates and C_2H_6/C_2H_4 yields.[85,107] It was proposed that C−H bond activation can be mediated by either surface atomic oxygen species or by surface OH radicals, and that the greater reactivity was related to the presence of the more reactive surface OH radicals.

6. PROPOSED CATALYTIC OCM REACTION MECHANISMS

The C−H bond dissociation energy of CH_4 is 439.3 kJ/mol reflecting the strong C−H bonds of methane.[3] The high stability of the C−H bonds in the CH_4 molecule stems from its tetrahedral (T_d) geometry where the central carbon is sp^3 hybridized with four hydrogen atoms. The resulting HOMO−LUMO gap makes it extremely hard to donate an electron into the LUMO or abstract one from the HOMO to activate the molecule.[108] If the catalyst surface interacts with a CH_4 molecule, however, its T_d geometry can be lowered.[108] The decrease in the C−H bond order of CH_4 would physically be interpreted as elongation (weakening) of the C−H bonds leading to the distortion of the T_d geometry, with the weakened C−H bond ultimately breaking, yielding a methyl radical (CH_3·).[108]

In the presence of a catalyst, methyl radical generation can take place via heterolytic cleavage that requires transfer of an electron between the activated oxygen species at the catalyst surface and the adsorbing methane molecule.[3] Therefore, an electron-acceptor catalyst (reducible, Lewis acid) would be required to activate adsorption of CH_4 to form CH_3·, and an electron donor (oxidizable, Lewis base) would be needed to activate gas phase molecular O_2 on the catalyst surface, which is crucial for conducting the OCM reaction. It has been repeatedly demonstrated that the OCM mechanism involves gaseous CH_3· radicals that recombine to form C_2H_6.[29,109,110]

Two proposed catalytic OCM reaction mechanisms have received the most attention in the catalysis literature. One of the very first and the most widely known OCM mechanism was proposed by Lunsford et al. in 1995.[29] The Lunsford mechanism for OCM by supported $Na/Mn_2O_3/SiO_2$ (depicted below in Figure 2) initially involves activation of gas phase molecular O_2 by dissociative adsorption at the Na sites followed by activation of the methane C−H bond by the formed surface oxygen atoms on the catalytic active Na sites, which leads to the initial formation of gas phase CH_3· radicals. This was confirmed for supported $Mn/Na_2WO_4/SiO_2$ and $Mn/Na_2WO_4/MgO$ catalysts with matrix isolation electron spin resonance (MI-ESR) measurements at both low ($P_{(total)}$ = 1 Torr) and high pressures ($P_{(total)}$ = 760 Torr) with the CH_3· radicals subsequently recombining to form C_2H_6.[29,84,111] Lunsford et al. also concluded that the OCM reaction proceeded via the same mechanism on both supported $Mn/Na_2WO_4/SiO_2$ and $Mn/Na_2WO_4/MgO$ catalysts. The similar conversion and selectivity properties of the two catalysts

DOI: 10.1021/acscatal.9b01585
ACS Catal. 2019, 9, 5912−5928

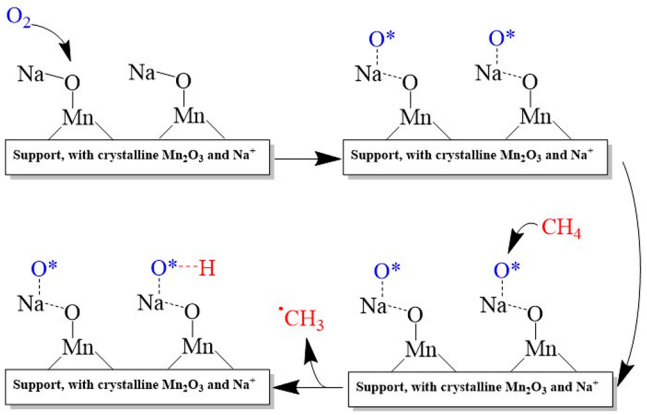

Figure 2. Catalytic OCM reaction mechanism proposed by Lunsford et al., where the active site is comprised of a Na−O−Mn bond, and WO_4 is only suggested as a stabilizer to prevent sintering/deactivation.[24]

suggested that WO_x centers were not active in the OCM reaction.[24]

The second widely cited OCM reaction mechanism for the supported $Mn_2O_3/Na_2WO_4/SiO_2$ catalyst was initially proposed by Li et al.[26,30] and later by Wang et al.[59,111] According to this mechanism (depicted below in Figure 3), two different active metal oxide sites work in unison. The CH_4 molecule is activated by the surface lattice oxygen associated with the surface WO_4 (W^{6+}) site that generates a gaseous methyl radical and reduces the surface WO_x site ($W^{6+} \rightarrow W^{5+}$).[30] This is

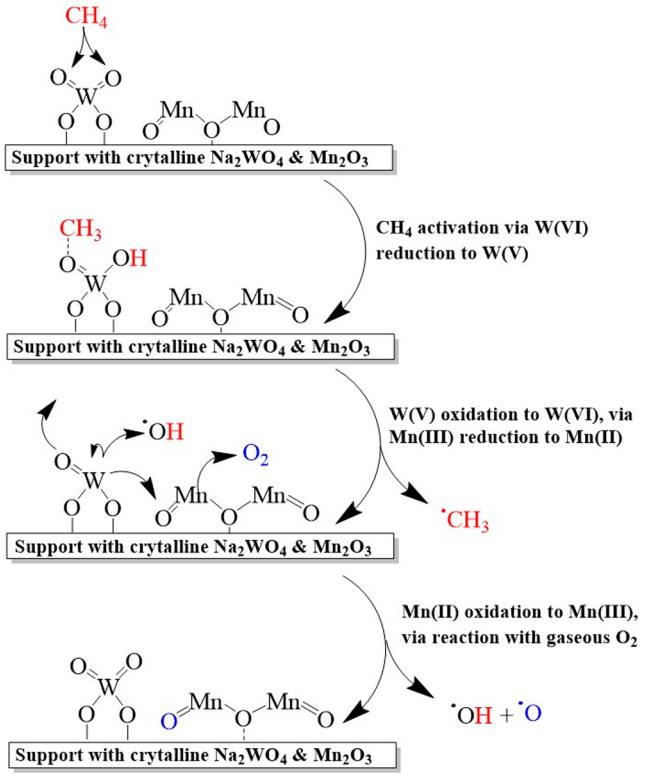

Figure 3. Catalytic OCM mechanism proposed by Li et al. where Na-coordinated WO_4 is the methyl generating active site, while a Mn_2O_3 in the neighborhood is responsible for gas phase activation. This mechanism and modified versions of it are widely accepted/discussed in the literature.[26,30,48,59,111]

accompanied by an electron transfer from W^{5+} to Mn^{3+}, which regenerates the W^{6+} site and reduces Mn^{3+} to Mn^{2+}.[30] The Mn^{2+} is then involved in the activation of gas phase molecular O_2 to form surface oxygen species via electron donation, which again generates a Mn^{3+} site. Supporting evidence for the molecular structures of the surface active sites and multiple reaction steps, however, has not been provided. Thus, this mechanism is highly speculative.

It is also important to note that, although OCM has traditionally been modeled as a heterogeneous catalytic process, at temperatures greater than 600 °C, homogeneous gas-phase reactions become relevant.[15] At such high temperatures, homogeneous reactions can produce ethylene and ethane from methane even without any catalyst, oxidize desired products, and even lead to steam reformation of CH_4. The extent of such homogeneous reactions depends strongly on residence times, CH_4/O_2 ratio and reactor pressure.[22]

The involvement of the active oxygen species during the OCM reaction over $Mn/Na_2WO_4/SiO_2$ catalyst was recently elucidated by Gordienko et al.,[79] who studied this catalyst using O_2-temperature-programmed desorption (O_2-TPD), pulse reduction−oxidation, and thermal gravimetric analysis-mass spectroscopy (TGA-MS). It was found that two different kinds of lattice oxygen were present: strongly adsorbed oxygen and weakly adsorbed oxygen. The weakly adsorbed and highly reactive surface lattice oxygen was linked to selective oxidation or the production of C_2 products, while strongly adsorbed oxygen species was associated with leading to full oxidation or CO_2 production. Another recent study on the role of oxygen by Fleischer et al.[97] applied H_2-TPR, O_2-TPD, and temperature-programmed surface reaction (TPSR). The surface oxygen population density was found to be 17 O* atoms/nm^2 that is much higher than typical monolayer coverages (0.1−10 O* atoms/nm^2)[97] on supported transition metal oxide surfaces.[112] Moreover, O_2-TPD measurements showed that two desorption peaks at 277 °C from weakly adsorbed oxygen and at 727 °C from strongly adsorbed oxygen. Lastly, the TPSR results in conjunction with simulation results were used to show that in the absence of gas-phase molecular O_2 two different lattice oxygen species were involved in the OCM reaction: electrophilic lattice oxygen producing C_2 products and nucleophilic lattice oxygen producing CO_2. Most recent studies are in agreement with the findings of Fleischer et al. and Gordienko et al. that exchange of gas-phase O_2 with lattice oxygen and the participation of at least two types of lattice oxygen species in the OCM reaction.

7. CATALYST STABILITY AND DEACTIVATION

The supported Mn_2O_3−Na_2WO_4/SiO_2 catalysts were found to be stable (almost constant performance) for extended time on stream (450−1000 h) during the OCM reaction in fixed-bed and fluid-bed reactor studies at temperatures of 800−875 °C.[113,114] Other studies have also reported this catalyst to be stable, although for a relatively shorter reaction periods (15−100 h).[15,63,115,116]

8. SUMMARY AND RECOMMENDATIONS

The OCM literature about the nature of the catalytic active sites for supported $Mn/Na_2WO_4/SiO_2$ catalysts can be summarized as follows: (a) The supported $Mn/Na_2WO_4/SiO_2$ catalysts have been synthesized with numerous types of precursors, synthesis methods, and different types of SiO_2

DOI: 10.1021/acscatal.9b01585
ACS Catal. 2019, 9, 5912−5928

supports that can strongly affect the nature and structure of the final catalyst. Our analysis shows that using $Na_2WO_4{\cdot}2H_2O$ as a precursor leads to formation of only crystalline Na_2WO_4 in the final catalyst, which can be avoided if individual precursors like NaOH, ammonium meta/para-tungstate are used. (Tables 1 and 2) The IWI prepared catalysts are the most commonly employed and have exhibited thermal stability during the OCM reaction. The OCM literature lacks detailed characterization of the catalysts synthesized by methods other than IWI, summarized in Tables 1 and 2. (b)The supported Mn/Na_2WO_4/SiO_2 catalysts are highly dynamic and their structures depend on environmental conditions (see Table 2). Under ambient conditions, the crystalline phases of Na_2WO_4, $Na_2W_2O_7$, Mn_2O_3, $MnWO_4$, and SiO_2 (α-cristobalite) phases can be present. Under OCM reaction conditions, the only crystalline phase present is the SiO_2 (β-cristobalite) support since the other crystalline phases become molten at such high temperatures (>750 °C).[33] (Table 2). (c) The crystalline phases detected under ambient conditions are not the catalytic active sites for OCM since they are not present under OCM reaction conditions. (d) The transformation of the initial amorphous SiO_2 support to crystalline SiO_2 (cristobalite) is accelerated by the presence of Na that lowers the transition temperature from ∼1500 °C to ∼750 °C.[63,69−72] (e) Information about surface metal oxide sites under all environmental conditions, especially under OCM reaction conditions from in situ and operando spectroscopic characterization, is still absent from the OCM literature. This deficiency makes any proposed structure−activity relationships highly speculative since the contribution of surface sites to the OCM reaction is still not known.[5466,79] (f) There is a synergy between all three active metal oxides (MnO_x, WO_x, and NaO_x) since the absence of any one of these components decreases the catalytic performance (C_2 hydrocarbon yield) (Figure 1). (g) The copresence of multiple active sites, molten phases, and surface phases requires a detailed investigation of the contribution of each component to the OCM catalytic reaction.[13,59,64] Speculated roles of each metal oxide component (Table 3) can only be understood and validated once model catalyst systems are thoroughly investigated with surface sensitive techniques at OCM relevant conditions.

The OCM catalytic literature about the reaction mechanism and kinetics can be summarized as follows: (a) The reaction pathways and kinetics of the catalytic OCM reaction are still not well understood because decoupling the contributions of gas-phase reactions from surface reactions has not yet been well established. (b) The activation of the gas phase CH_4 reactant's C−H bond upon adsorption is the rate-determining step, which was demonstrated by the presence of a kinetic isotope effect. (c) The resulting $CH_3{\cdot}$ radicals subsequently desorbs into the gas-phase to couple and form C_2H_6. (d) The formed C_2H_6 can further undergo dehydrogenation both in the gas-phase and on the catalyst surface via ethyl intermediates to form C_2H_4. (e) All hydrocarbons (CH_4, C_2H_6, and C_2H_4) can be overoxidized to CO_x. Oxidation to CO dominates in the gas-phase and oxidation to CO_2 dominates on the catalyst surface. (f) Activation of CH_4 involves surface O* on the catalyst that is in equilibrium with both gas-phase molecular O_2 (Langmuir−Hinshelwood mechanism) and the catalyst bulk lattice oxygen (Mars−van Krevelen mechanism). (g) The OCM reaction kinetics is first-order in the partial pressure of CH_4 and 1/2-order in the partial pressure of O_2. The first-order dependence in CH_4 indicates the participation of molecular CH_4 in the rate-determining-step. The 1/2-order in O_2 reflects the participation of surface atomic oxygen (O*) in the rate-determining-step. (h) The reported kinetic parameters for activation of CH_4, C_2H_6, and C_2H_4 differ widely, and no consensus has been reached on the kinetic parameters.

Further advancement of the fundamental structure−activity relationships of the OCM catalytic reaction that will guide the rational design of improved catalysts will require the following: (a) in situ and operando spectroscopy studies under OCM reaction conditions to determine the structure and catalytic contribution of crystalline, molten, and surface phases (e.g., W/SiO_2, Mn/SiO_2, Na/SiO_2, $Mn−W/SiO_2$, $Mn−Na/SiO_2$, $W−Na/SiO_2$, and $Mn−W−Na/SiO_2$). (b) Synthesize model SiO_2-supported catalysts containing only surface oxide sites (MnO_x, WO_x, NaO_x, $MnO_x−NaO_x$, $MnO_x−WO_x$ sites, $MnO_x−WO_x−NaO_x$) and determine their structure−activity/selectivity properties and contribution for OCM. (c) Isotopic $^{12}C−^{13}C$ hydrocarbons (e.g., $^{12}CH_4/^{13}C_2H_6$, $^{12}CH_4/^{13}C_2H_4$, and $^{12}C_2H_4/^{13}C_2H_6$) and $^{16}O−^{18}O$ studies (e.g., $^{16}O_2−^{18}O_2$) to determine the relative kinetics among the participating hydrocarbons and assist in decoupling the gas-phase and surface reactions. (d) Temporal analysis of products (TAP) experiments within Knudsen diffusion limit will completely eliminate gas-phase reactions and only allow the surface catalyzed reactions to proceed. (e) Transient experiments (SSITKA, TPSR, and pulse experiments) to determine the number of participating active oxygen sites (surface O*), TOF values, and intrinsic kinetic parameters from pulse experiments with very small pulse size (oxidation of CH_4, C_2H_4, and C_2H_6) and redox reaction steps. (f) Determine the redox kinetics of the WO_x and MnO_x sites with in situ and operando Raman, UV−vis, and quick XANES spectroscopy.

AUTHOR INFORMATION

Corresponding Authors

*E-mail: job314@lehigh.edu.

*E-mail: iew0@lehigh.edu.

ORCID

Jonas Baltrusaitis: 0000-0001-5634-955X

Israel E. Wachs: 0000-0001-5282-128X

Author Contributions

‡D.K. and S.S. contributed equally.

Notes

The authors declare no competing financial interest.

ACKNOWLEDGMENTS

This work is supported by NSF CBET 1706581. The authors also gratefully acknowledge insightful input from Dr. Michael E. Ford of the *Operando* Molecular Spectroscopy and Catalysis Laboratory at Lehigh University, Professor Oz Gazit and Naseem Hayek of Technion, Israel. Professor I.E. Wachs gratefully acknowledges the support of Fulbright USA-Israel for the Fulbright Senior Scholar Fellowship during his stay at Technion while writing this paper.

REFERENCES

(1) Horn, R.; Schlögl, R. Methane Activation by Heterogeneous Catalysis. *Catal. Lett.* **2015**, *145*, 23−39.

(2) Galadima, A.; Muraza, O. Revisiting the Oxidative Coupling of Methane to Ethylene in the Golden Period of Shale Gas: A Review. *J. Ind. Eng. Chem.* **2016**, *37*, 1−13.

DOI: 10.1021/acscatal.9b01585
ACS Catal. 2019, 9, 5912−5928

(3) Schwach, P.; Pan, X.; Bao, X. Direct Conversion of Methane to Value-Added Chemicals over Heterogeneous Catalysts: Challenges and Prospects. *Chem. Rev.* **2017**, *117*, 8497−8520.
(4) Chakrabarti, A.; Ford, M. E.; Gregory, D.; Hu, R.; Keturakis, C. J.; Lwin, S.; Tang, Y.; Yang, Z.; Zhu, M.; Banares, M. A.; Wachs, I. E. A Decade+ of Operando Spectroscopy Studies. *Catal. Today* **2017**, *283*, 27−53.
(5) Ma, S.; Guo, X.; Zhao, L.; Scott, S.; Bao, X. Recent Progress in Methane Dehydroaromatization: From Laboratory Curiosities to Promising Technology. *J. Energy Chem.* **2013**, *22*, 1−20.
(6) Guo, X.; Fang, G.; Li, G.; Ma, H.; Fan, H.; Yu, L.; Ma, C.; Wu, X.; Deng, D.; Wei, M.; Tan, D.; Si, R.; Zhang, S.; Li, J.; Tang, Z.; Pan, X.; Bao, X.; Sun, L. Direct, Nonoxidative Conversion of Methane to Ethylene, Aromatics, and Hydrogen. *Science* **2014**, *344*, 616−619.
(7) Huang, K.; Miller, J. B.; Huber, G. W.; Dumesic, J. A.; Maravelias, C. T. A General Framework for the Evaluation of Direct Nonoxidative Methane Conversion Strategies. *Joule* **2018**, *2*, 349−365.
(8) Lomonosov, V. I.; Sinev, M. Y. Oxidative Coupling of Methane: Mechanism and Kinetics. *Kinet. Catal.* **2016**, *57*, 647−676.
(9) Sinev, M. Y.; Fattakhova, Z. T.; Lomonosov, V. I.; Gordienko, Y. A. Kinetics of Oxidative Coupling of Methane: Bridging the Gap between Comprehension and Description. *J. Nat. Gas Chem.* **2009**, *18*, 273−287.
(10) Fan, D.; Dai, D.; Wu, H. Ethylene Formation by Catalytic Dehydration of Ethanol with Industrial Considerations. *Materials* **2013**, *6*, 101−115.
(11) Keller, G. E.; Bhasin, M. M. Synthesis of Ethylene via Oxidative Coupling of Methane: I. Determination of Active Catalysts. *J. Catal.* **1982**, *73*, 9−19.
(12) Arndt, S.; Otremba, T.; Simon, U.; Yildiz, M.; Schubert, H.; Schomäcker, R. Mn-Na2WO4/SiO2 as Catalyst for the Oxidative Coupling of Methane. What Is Really Known? *Appl. Catal., A* **2012**, *425*−*426*, 53−61.
(13) Wang, P.; Zhao, G.; Wang, Y.; Lu, Y. MnTiO3-Driven Low-Temperature Oxidative Coupling of Methane over TiO2-Doped Mn2O3-Na2WO4/SiO2catalyst. *Sci. Adv.* **2017**, *3*, e1603180.
(14) Wang, D. J.; Rosynek, M. P.; Lunsford, J. H. Oxidative Coupling of Methane over Oxide-Supported Sodium-Manganese Catalysts. *J. Catal.* **1995**, *155*, 390−402.
(15) Pak, S.; Qiu, P.; Lunsford, J. H. Elementary Reactions in the Oxidative Coupling of Methane over Mn/Na2WO4/SiO2 and Mn /Na2WO4/MgO Catalysts. *J. Catal.* **1998**, *179*, 222−230.
(16) Daneshpayeh, M.; Khodadadi, A.; Mostoufi, N.; Mortazavi, Y.; Sotudeh-Gharebagh, R.; Talebizadeh, A. Kinetic Modeling of Oxidative Coupling of Methane over Mn/Na2WO4/SiO2 Catalyst. *Fuel Process. Technol.* **2009**, *90*, 403−410.
(17) Wang, B.; Albarracín-Suazo, S.; Pagán-Torres, Y.; Nikolla, E. Advances in Methane Conversion Processes. *Catal. Today* **2017**, *285*, 147−158.
(18) Sinev, M. Y.; Margolis, L. Y.; Bychkov, V. Y.; Korchak, V. N. Free Radicals as Intermediates in Oxidative Transformations of Lower Alkanes. In *3rd World Congress on Oxidation Catalaysis*; Grasselli, R. K., Oyama, S. T., Gaffney, A. M., Lyons, J. E. B. T.-S., Eds.; Elsevier, 1997; Vol. *110*, 327−335.
(19) Lunsford, J. H. Catalytic Conversion of Methane to More Useful Chemicals and Fuels:A Challenge for the 21st Century. *Catal. Today* **2000**, *63*, 165−174.
(20) Farrell, B. L.; Igenegbai, V. O.; Linic, S. A Viewpoint on Direct Methane Conversion to Ethane and Ethylene Using Oxidative Coupling on Solid Catalysts. *ACS Catal.* **2016**, *6*, 4340−4346.
(21) Taifan, W.; Baltrusaitis, J. CH4 Conversion to Value Added Products: Potential, Limitations and Extensions of a Single Step Heterogeneous Catalysis. *Appl. Catal., B* **2016**, *198*, 525−547.
(22) Karakaya, C.; Kee, R. J. Progress in the Direct Catalytic Conversion of Methane to Fuels and Chemicals. *Prog. Energy Combust. Sci.* **2016**, *55*, 60−97.
(23) Palermo, A.; Holgado Vazquez, J. P.; Lee, A. F.; Tikhov, M. S.; Lambert, R. M. Critical Influence of the Amorphous Silica-to-Cristobalite Phase Transition on the Performance of Mn/Na2WO4/SiO2 Catalysts for the Oxidative Coupling of Methane. *J. Catal.* **1998**, *177*, 259−266.
(24) Pak, S.; Lunsford, J. H. Thermal Effects during the Oxidative Coupling of Methane over Mn/Na2WO4/SiO2 and Mn/Na2WO4/MgO Catalysts. *Appl. Catal., A* **1998**, *168*, 131−137.
(25) Luo, L.; Jin, Y.; Pan, H.; Zheng, X.; Wu, L.; You, R.; Huang, W. Distribution and Role of Li in Li-Doped MgO Catalysts for Oxidative Coupling of Methane. *J. Catal.* **2017**, *346*, 57−61.
(26) Wu, J.; Li, S. The Role of Distorted W04 in the Oxidative Coupling of Methane on Tungsten Oxide Supported Catalysts. *J. Phys. Chem.* **1995**, *99*, 4566−4568.
(27) Palermo, A.; Holgado Vazquez, J. P.; Lambert, R. M. New Efficient Catalysts for the Oxidative Coupling of Methane. *Catal. Lett.* **2000**, *68*, 191−196.
(28) Schwach, P.; Willinger, M. G.; Trunschke, A.; Schlögl, R. Methane Coupling over Magnesium Oxide: How Doping Can Work. *Angew. Chem., Int. Ed.* **2013**, *52*, 11381−11384.
(29) Lunsford, J. H. The Catalytic Oxidative Coupling of Methane. *Angew. Chem., Int. Ed. Engl.* **1995**, *34*, 970−980.
(30) Li, S.-B. Oxidative Coupling of Methane over W-Mn/SiO2 Catalyst. *Chin. J. Chem.* **2001**, *19*, 16−21.
(31) Wang, J.; Chou, L.; Zhang, B.; Song, H.; Zhao, J.; Yang, J.; Li, S. Comparative Study on Oxidation of Methane to Ethane and Ethylene over Na2WO4-Mn/SiO2catalysts Prepared by Different Methods. *J. Mol. Catal. A: Chem.* **2006**, *245*, 272−277.
(32) Lwin, S.; Li, Y.; Frenkel, A. I.; Wachs, I. E. Nature of WOx Sites on SiO2and Their Molecular Structure-Reactivity/Selectivity Relationships for Propylene Metathesis. *ACS Catal.* **2016**, *6*, 3061−3071.
(33) Vamvakeros, A.; Jacques, S. D. M.; Middelkoop, V.; Di Michiel, M.; Egan, C. K.; Ismagilov, I. Z.; Vaughan, G. B. M.; Gallucci, F.; van Sint Annaland, M.; Shearing, P. R.; Cernik, R. J.; Beale, A. M. Real Time Chemical Imaging of a Working Catalytic Membrane Reactor during Oxidative Coupling of Methane. *Chem. Commun.* **2015**, *51*, 12752−12755.
(34) Wachs, I. E.; Roberts, C. A. Monitoring Surface Metal Oxide Catalytic Active Sites with Raman Spectroscopy. *Chem. Soc. Rev.* **2010**, *39*, 5002.
(35) Strunk, J.; Bañares, M. A.; Wachs, I. E. Vibrational Spectroscopy of Oxide Overlayers. *Top. Catal.* **2017**, *60*, 1577−1617.
(36) Bravo-Suárez, J. J.; Srinivasan, P. D. Design Characteristics of in Situ and Operando Ultraviolet-Visible and Vibrational Spectroscopic Reaction Cells for Heterogeneous Catalysis. *Catal. Rev.: Sci. Eng.* **2017**, *00*, 1−151.
(37) Beale, A. M.; Van Der Eerden, A. M. J.; Kervinen, K.; Newton, M. A.; Weckhuysen, B. M. Adding a Third Dimension to Operando Spectroscopy: A Combined UV-Vis, Raman and XAFS Setup to Study Heterogeneous Catalysts under Working Conditions. *Chem. Commun.* **2005**, *24*, 3015−3017.
(38) Weckhuysen, B. M. Determining the Active Site in a Catalytic Process: Operando Spectroscopy Is More than a Buzzword. *Phys. Chem. Chem. Phys.* **2003**, *5*, 4351−4360.
(39) Vamvakeros, A. Operando Chemical Tomography of Packed Bed and Membrane Reactors for Methane Processing. Thesis, Department of Chemistry, University College London, 2017.
(40) Taifan, W. E.; Li, Y.; Baltrus, J. P.; Zhang, L.; Frenkel, A. I.; Baltrusaitis, J. Operando Structure Determination of Cu and Zn on Supported MgO/SiO_2 Catalysts during Ethanol Conversion to 1,3-Butadiene. *ACS Catal.* **2019**, *9*, 269−285.
(41) Zhu, M.; Li, B.; Jehng, J.-M. M.; Sharma, L.; Taborda, J.; Zhang, L.; Stach, E.; Wachs, I. E.; Wu, Z.; Baltrusaitis, J. Molecular Structure and Sour Gas Surface Chemistry of Supported $K_2O/WO_3/Al_2O_3$ catalysts. *Appl. Catal., B* **2018**, *232*, 146−154.
(42) Lee, E. L.; Wachs, I. E. In Situ Spectroscopic Investigation of the Molecular and Electronic Structures of SiO2 Supported Surface Metal Oxides. *J. Phys. Chem. C* **2007**, *111*, 14410−14425.
(43) Taifan, W. E.; Yan, G. X.; Baltrusaitis, J. Surface Chemistry of MgO/SiO_2 catalyst during the Ethanol Catalytic Conversion to 1,3-

DOI: 10.1021/acscatal.9b01585
ACS Catal. 2019, 9, 5912−5928

Butadiene: In-Situ DRIFTS and DFT Study. *Catal. Sci. Technol.* **2017**, *7*, 4648−4668.
(44) Taifan, W. E.; Baltrusaitis, J. In Situ Spectroscopic Insights on the Molecular Structure of the MgO/SiO_2 Catalytic Active Sites during Ethanol Conversion to 1,3-Butadiene. *J. Phys. Chem. C* **2018**, *122*, 20894−20906.
(45) Weckhuysen, B. M.; Jehng, J.-M.; Wachs, I. E. In Situ Raman Spectroscopy of Supported Transition Metal Oxide Catalysts: $^{18}O_2$−$^{16}O_2$ Isotopic Labeling Studies. *J. Phys. Chem. B* **2000**, *104*, 7382−7387.
(46) Bañares, M. A.; Martínez-Huerta, M. V.; Gao, X.; Fierro, J. L. G.; Wachs, I. E. Dynamic Behavior of Supported Vanadia Catalysts in the Selective Oxidation of Ethane. In Situ Raman, UV−vis DRS and Reactivity Studies. *Catal. Today* **2000**, *61*, 295−301.
(47) Yildiz, M.; Aksu, Y.; Simon, U.; Kailasam, K.; Goerke, O.; Rosowski, F.; Schomäcker, R.; Thomas, A.; Arndt, S. Enhanced Catalytic Performance of Mn_xO_y−Na_2WO_4/SiO_2 for the Oxidative Coupling of Methane Using an Ordered Mesoporous Silica Support. *Chem. Commun.* **2014**, *50*, 14440−14442.
(48) Hayek, N. S.; Lucas, N. S.; Warwar Damouny, C.; Gazit, O. M. Critical Surface Parameters for the Oxidative Coupling of Methane over the Mn−Na−W/SiO_2 Catalyst. *ACS Appl. Mater. Interfaces* **2017**, *9*, 40404−40411.
(49) Ismagilov, I. Z.; Matus, E. V.; Kuznetsov, V. V.; Kerzhentsev, M. A.; Yashnik, S. A.; Larina, T. V.; Prosvirin, I. P.; Navarro, R. M.; Fierro, J. L. G.; Gerritsen, G.; Abbenhuis, H. C.; Ismagilov, R. Z. Effect of Preparation Mode on the Properties of Mn-Na-W/SiO_2 catalysts for Oxidative Coupling of Methane: Conventional Methods vs. POSS Nanotechnology. *Eurasian Chem.-Technol. J.* **2016**, *18*, 93−110.
(50) Grant, J. T.; Carrero, C. A.; Love, A. M.; Verel, R.; Hermans, I. Enhanced Two-Dimensional Dispersion of Group v Metal Oxides on Silica. *ACS Catal.* **2015**, *5*, 5787−5793.
(51) Wu, J.; Ramanathan, A.; Biancardi, A.; Jystad, A.; Caricato, M.; Hu, Y.; Subramaniam, B. Correlation Of Active Site Precursors And Olefin Metathesis Activity In W-Incorporated Silicates. *ACS Catal.* **2018**, *8*, 10437−10445.
(52) Carrero, C. A.; Schloegl, R.; Wachs, I. E.; Schomaecker, R. Critical Literature Review of the Kinetics for the Oxidative Dehydrogenation of Propane over Well-Defined Supported Vanadium Oxide Catalysts. *ACS Catal.* **2014**, *4*, 3357−3380.
(53) Kiani, D.; Belletti, G.; Quaino, P.; Tielens, F.; Baltrusaitis, J. Structure and Vibrational Properties of Potassium-Promoted Tungsten Oxide Catalyst Monomeric Sites Supported on Alumina ($K_2O/WO_3/Al_2O_3$) Characterized Using Periodic Density Functional Theory. *J. Phys. Chem. C* **2018**, *122*, 24190−24201.
(54) Ji, S.; Xiao, T.; Li, S.; Chou, L.; Zhang, B.; Xu, C.; Hou, R.; York, A. P. E.; Green, M. L. H. Surface WO_4 tetrahedron: The Essence of the Oxidative Coupling of Methane over M-W-Mn/SiO_2 catalysts. *J. Catal.* **2003**, *220*, 47−56.
(55) Sugiura, K.; Ogo, S.; Iwasaki, K.; Yabe, T.; Sekine, Y. Low-Temperature Catalytic Oxidative Coupling of Methane in an Electric Field over a Ce-W-O Catalyst System. *Sci. Rep.* **2016**, *6*, 3−4.
(56) Jiang, Z. C.; Yu, C. J.; Fang, X. P.; Li, S. B.; Wang, H. L. Oxide/Support Interaction and Surface Reconstruction in the Sodium Tungstate(Na_2WO_4)/Silica System. *J. Phys. Chem.* **1993**, *97*, 12870−12875.
(57) Wu, J.; Li, S.; Niu, J.; Fang, X. Mechanistic Study of Oxidative Coupling of Methane over Mn_2O_3-Na_2WO_4/SiO_2 Catalyst. *Appl. Catal., A* **1995**, *124*, 9−18.
(58) Ji, S.; Xiao, T.; Li, S.; Xu, C.; Hou, R.; Coleman, K. S.; Green, M. L. H. The Relationship between the Structure and the Performance of Na-W-Mn/SiO_2 Catalysts for the Oxidative Coupling of Methane. *Appl. Catal., A* **2002**, *225* (1−2), 271−284.
(59) Wang, P.; Zhao, G.; Liu, Y.; Lu, Y. TiO_2-Doped Mn_2O_3−Na_2WO_4/SiO_2 Catalyst for Oxidative Coupling of Methane: Solution Combustion Synthesis and $MnTiO_3$-Dependent Low-Temperature Activity Improvement. *Appl. Catal., A* **2017**, *544*, 77−83.
(60) Godini, H. R.; Gili, A.; Görke, O.; Arndt, S.; Simon, U.; Thomas, A.; Schomäcker, R.; Wozny, G. Sol−Gel Method for Synthesis of Mn-Na_2WO_4/SiO_2 catalyst for Methane Oxidative Coupling. *Catal. Today* **2014**, *236*, 12−22.
(61) Fang, X.; Li, S.; Lin, J.; Chu, Y. Oxidative Coupling of Methane on W-Mn Catalysts. *J. Mol. Catal.* **1992**, *6*, 427−433.
(62) Fang, X. P.; Li, S. B.; Lin, J. Z.; Gu, J. F.; Yang, D. X. Preparation and Characterization of W-Mn Catalyst for Oxidative Coupling of Methane. *J. Mol. Catal.* **1992**, *6*, 255−262.
(63) Simon, U.; Görke, O.; Berthold, A.; Arndt, S.; Schomäcker, R.; Schubert, H. Fluidized Bed Processing of Sodium Tungsten Manganese Catalysts for the Oxidative Coupling of Methane. *Chem. Eng. J.* **2011**, *168*, 1352−1359.
(64) Riedel, W.; Thum, L.; Möser, J.; Fleischer, V.; Simon, U.; Siemensmeyer, K.; Schnegg, A.; Schomäcker, R.; Risse, T.; Dinse, K.-P. Magnetic Properties of Reduced and Reoxidized Mn−Na_2WO_4/SiO_2 : A Catalyst for Oxidative Coupling of Methane (OCM). *J. Phys. Chem. C* **2018**, *122*, 22605−22614.
(65) Ghose, R.; Hwang, H. T.; Varma, A. Oxidative Coupling of Methane Using Catalysts Synthesized by Solution Combustion Method: Catalyst Optimization and Kinetic Studies. *Appl. Catal., A* **2014**, *472*, 39−46.
(66) Koirala, R.; Büchel, R.; Pratsinis, S. E.; Baiker, A. Oxidative Coupling of Methane on Flame-Made Mn-Na_2WO_4/SiO_2: Influence of Catalyst Composition and Reaction Conditions. *Appl. Catal., A* **2014**, *484*, 97−107.
(67) Li, S. Reaction Chemistry of W-Mn/SiO_2 Catalyst for the Oxidative Coupling of Methane. *J. Nat. Gas Chem.* **2003**, *12*, 1−9.
(68) Ji, S.; Xiao, T.; Li, S.; Xu, C.; Hou, R.; Coleman, K. S.; Green, M.; Wu, J.; Jiang, Z. C. Oxidative Coupling of Methane over Oxide-Supported Sodium-Manganese Catalysts. *Appl. Catal. A Gen.* **1995**, *68*, 191−196.
(69) Hou, S.; Cao, Y.; Xiong, W.; Liu, H.; Kou, Y. Site Requirements for the Oxidative Coupling of Methane on SiO_2-Supported Mn Catalysts. *Ind. Eng. Chem. Res.* **2006**, *45*, 7077−7083.
(70) Hatch, D. M.; Ghose, S. The A-β Phase Transition in Cristobalite, SiO_2.Pdf. *Phys. Chem. Miner.* **1991**, *17*, 554−562.
(71) Meike, A.; Glassley, W. E. *In-Situ Observation of the Alpha/Beta Cristobalite Transition Using High Voltage Electron Microscopy*; Materials Research Society: United States, 1990.
(72) Damby, D. E.; Llewellin, E. W.; Horwell, C. J.; Ben, J.; et al. The α−β Phase Transition in Volcanic Cristobalite Research Papers. *J. Appl. Crystallogr.* **2014**, *47*, 1205−1215.
(73) Goodenough, J. B.; Hamnett, A.; Huber, G.; Hullinger, F.; Leiß, M.; Ramasesha, S. K.; Werheit, H. *Physics of Non-Tetrahedrally Bonded Binary Compounds III/Physik Der Nicht-Tetraedrisch Gebundenen Binären Verbindungen III*; Madelung, O., Ed.; Springer-Verlag Berlin Heidelberg, 1984.
(74) Stobbe, E. R.; de Boer, B. A.; Geus, J. W. Reduction and Oxidation Behaviour of Manganese Oxides. *Catal. Today* **1999**, *47*, 161−167.
(75) Yang, T.; Feng, L.; Shen, S. Oxygen Species on the Surface of La_2O_3/CaO and Its Role in the Oxidative Coupling of Methane. *J. Catal.* **1994**, *145*, 384−389.
(76) Kou, Y.; Zhang, B.; Niu, J.; Li, S.; Wang, H.; Tanaka, T.; Yoshida, S. Amorphous Features of Working Catalysts: XAFS and XPS Characterization of $Mn/Na_2WO_4/SiO_2$ as Used for the Oxidative Coupling of Methane. *J. Catal.* **1998**, *173*, 399−408.
(77) Wang, X.; Zhang, J.; Yang, D.; Zhang, C.; Lin, J.; Li, S. Oxidative Coupling of Methane over W-Mn/SiO_2 Catalyst in a Bench-Scale Stainless Steel Fluidized-Bed Reactor. *Petrochem. Technol.* **1997**, *26*, 272−277.
(78) Yildiz, M.; Aksu, Y.; Simon, U.; Otremba, T.; Kailasam, K.; Göbel, C.; Girgsdies, F.; Görke, O.; Rosowski, F.; Thomas, A.; Schomäcker, R.; Arndt, S. Silica Material Variation for the Mn_xO_y-Na_2WO_4/SiO_2. *Appl. Catal., A* **2016**, *525*, 168−179.
(79) Gordienko, Y.; Usmanov, T.; Bychkov, V.; Lomonosov, V.; Fattakhova, Z.; Tulenin, Y.; Shashkin, D.; Sinev, M. Oxygen Availability and Catalytic Performance of $NaWMn/SiO_2$ mixed

DOI: 10.1021/acscatal.9b01585
ACS Catal. 2019, 9, 5912−5928

Oxide and Its Components in Oxidative Coupling of Methane. *Catal. Today* **2016**, *278*, 127−134.
(80) Arndt, S.; Otremba, T.; Simon, U.; Yildiz, M.; Schubert, H.; Schomäcker, R. Mn−Na_2WO_4/SiO_2 as Catalyst for the Oxidative Coupling of Methane. What Is Really Known? *Appl. Catal., A* **2012**, *425*−*426*, 53−61.
(81) Ross-medgaarden, E. I.; Wachs, I. E. Structural Determination of Bulk and Surface Tungsten Oxides with UV−vis Diffuse Reflectance Spectroscopy and Raman Spectroscopy. *J. Phys. Chem. C* **2007**, *111*, 15089−15099.
(82) Kim, D. S.; Ostromecki, M.; Wachs, I. E.; Kohler, S. D.; Ekerdt, J. G. *Catal. Lett.* **1995**, *33*, 209−215.
(83) Lee, E. L.; Wachs, I. E. In Situ Spectroscopic Investigation of the Molecular and Electronic Structures of SiO_2-Supported Surface Metal Oxides. *J. Phys. Chem. C* **2007**, *111*, 14410−14425.
(84) Pak, S.; Qiu, P.; Lunsford, J. H. Elementary Reactions in the Oxidative Coupling of Methane over Mn/Na_2WO_4/SiO_2 and Mn/Na_2WO_4/MgO Catalysts. *J. Catal.* **1998**, *179*, 222−230.
(85) Takanabe, K.; Iglesia, E. Mechanistic Aspects and Reaction Pathways for Oxidative Coupling of Methane on Mn/Na_2WO_4/SiO_2 Catalysts. *J. Phys. Chem. C* **2009**, *113*, 10131−10145.
(86) Tiemersma, T. P.; Tuinier, M. J.; Gallucci, F.; Kuipers, J. A. M.; van Sint Annaland, M. A Kinetics Study for the Oxidative Coupling of Methane on a Mn/Na_2WO_4/SiO_2 Catalyst. *Appl. Catal., A* **2012**, *433*−*434*, 96−108.
(87) Beck, B.; Fleischer, V.; Arndt, S.; Hevia, M. G.; Urakawa, A.; Hugo, P.; Schomäcker, R. Oxidative Coupling of Methane—A Complex Surface/Gas Phase Mechanism with Strong Impact on the Reaction Engineering. *Catal. Today* **2014**, *228*, 212−218.
(88) Lunsford, J. H. Formation and Reactions of Methyl Radicals over Metal Oxide Catalysts. In *Methane Conversion by Oxidative Processes*; Springer, 1992; pp 3−29.
(89) Tong, Y.; Lunsford, J. H. Gas-Phase Coupling of Methyl Radicals during the Partial Oxidation of Methane over Transition Metal Oxide Catalysts. *J. Chem. Soc., Chem. Commun.* **1990**, *792*, 792−793.
(90) Martir, W.; Lunsford, J. H. Formation of Gas-Phase. Pi.-Allyl Radicals from Propylene over Bismuth Oxide and. Gamma.-Bismuth Molybdate Catalysts. *J. Am. Chem. Soc.* **1981**, *103*, 3728−3732.
(91) Xu, M.; Ballinger, T. H.; Lunsford, J. H. Quantitative Studies of Methyl Radicals Reacting with Metal Oxides. *J. Phys. Chem.* **1995**, *99*, 14494−14499.
(92) Lomonosov, V. I.; Gordienko, Y. A.; Sinev, M. Y. Kinetics of the Oxidative Coupling of Methane in the Presence of Model Catalysts. *Kinet. Catal.* **2013**, *54*, 451−462.
(93) Dooley, S.; Burke, M. P.; Chaos, M.; Stein, Y.; Dryer, F. L.; Zhukov, V. P.; Finch, O.; Simmie, J. M.; Curran, H. J. Methyl Formate Oxidation: Speciation Data, Laminar Burning Velocities, Ignition Delay Times, and a Validated Chemical Kinetic Model. *Int. J. Chem. Kinet.* **2010**, *42*, 527−549.
(94) Schwarz, H.; Geske, M.; Franklin Goldsmith, C.; Schlögl, R.; Horn, R. Fuel-Rich Methane Oxidation in a High-Pressure Flow Reactor Studied by Optical-Fiber Laser-Induced Fluorescence, Multi-Species Sampling Profile Measurements and Detailed Kinetic Simulations. *Combust. Flame* **2014**, *161*, 1688−1700.
(95) Chen, Q.; Hoebink, J. H. B. J.; Marin, G. B. Kinetics of the Oxidative Coupling of Methane at Atmospheric Pressure in the Absence of Catalyst. *Ind. Eng. Chem. Res.* **1991**, *30*, 2088−2097.
(96) Chen, Q.; Couwenberg, P. M.; Marin, G. B. Effect of Pressure on the Oxidative Coupling of Methane in the Absence of Catalyst. *AIChE J.* **1994**, *40*, 521−535.
(97) Fleischer, V.; Steuer, R.; Parishan, S.; Schomäcker, R. Investigation of the Surface Reaction Network of the Oxidative Coupling of Methane over Na_2WO_4/Mn/SiO_2 Catalyst by Temperature Programmed and Dynamic Experiments. *J. Catal.* **2016**, *341*, 91−103.
(98) Thybaut, J. W.; Sun, J.; Olivier, L.; Van Veen, A. C.; Mirodatos, C.; Marin, G. B. Catalyst Design Based on Microkinetic Models: Oxidative Coupling of Methane. *Catal. Today* **2011**, *159*, 29−36.
(99) Shahri, S. M. K.; Alavi, S. M. Kinetic Studies of the Oxidative Coupling of Methane over the Mn/Na_2WO_4/SiO_2 Catalyst. *J. Nat. Gas Chem.* **2009**, *18*, 25−34.
(100) Lee, M. R.; Park, M.-J.; Jeon, W.; Choi, J.-W.; Suh, Y.-W.; Suh, D. J. A Kinetic Model for the Oxidative Coupling of Methane over Na_2WO_4/Mn/SiO_2. *Fuel Process. Technol.* **2012**, *96*, 175−182.
(101) Sadeghzadeh Ahari, J.; Zarrinpashne, S.; Sadeghi, M. T. Micro-Kinetic Modeling of OCM Reactions over Mn/Na_2WO_4/SiO_2 Catalyst. *Fuel Process. Technol.* **2013**, *115*, 79−87.
(102) Doornkamp, C.; Ponec, V. The Universal Character of the Mars and Van Krevelen Mechanism. *J. Mol. Catal. A: Chem.* **2000**, *162*, 19−32.
(103) Lin, C.-H.; Wang, J.-X.; Lunsford, J. H. Oxidative Dimerization of Methane over Sodium-Promoted Calcium Oxide. *J. Catal.* **1988**, *111*, 302−316.
(104) Ekstrom, A.; Regtop, R.; Bhargava, S. Effect of Pressure on the Oxidative Coupling Reaction of Methane. *Appl. Catal.* **1990**, *62*, 253−269.
(105) Ahari, J. S.; Sadeghi, M. T.; Zarrinpashne, S. Effects of Operating Parameters on Oxidative Coupling of Methane over Na-W-Mn/SiO_2 Catalyst at Elevated Pressures. *J. Nat. Gas Chem.* **2011**, *20*, 204−213.
(106) Sadeghzadeh Ahari, J.; Sadeghi, M. T.; Zarrinpashne, S.; Irandoukht, A. Optimization of OCM Reactions over Na−W−Mn/SiO_2 Catalyst at Elevated Pressure Using Artificial Neural Network and Response Surface Methodology. *Sci. Iran.* **2013**, *20* (3), 617−625.
(107) Takanabe, K.; Iglesia, E. Rate and Selectivity Enhancements Mediated by OH Radicals in the Oxidative Coupling of Methane Catalyzed by Mn/Na_2WO_4/SiO_2. *Angew. Chem.* **2008**, *120*, 7803−7807.
(108) Li, C.; Yan, W.; Xin, Q. Interaction of Methane with Surface of Alumina Studied by FT-IR Spectroscopy. *Catal. Lett.* **1994**, *24*, 249−256.
(109) Nelson, P. F.; Lukey, C. a.; Cant, N. W. Isotopic Evidence for Direct Methyl Coupling and Ethane to Ethylene Conversion during Partial Oxidation of Methane over Lithium/Magnesium Oxide. *J. Phys. Chem.* **1988**, *92*, 6176−6179.
(110) Mims, C. A.; Hall, R. B.; Rose, K. D.; Myers, G. R. Oxidative Dimerization of CH_4/CD_4 Mixtures: Evidence for Methyl Intermediate. *Catal. Lett.* **1989**, *2*, 361−368.
(111) Wang, P.; Zhao, G.; Liu, Y.; Lu, Y. TiO_2-Doped Mn_2O_3-Na_2WO_4/SiO_2 Catalyst for Oxidative Coupling of Methane: Solution Combustion Synthesis and $MnTiO_3$-Dependent Low-Temperature Activity Improvement. *Appl. Catal., A* **2017**, *544*, 77−83.
(112) Badlani, M.; Wachs, I. E. Methanol: A "Smart" Chemical Probe Molecule. *Catal. Lett.* **2001**, *75*, 137−149.
(113) Lin, J. Z.; Gu, J. F.; Yang, D. X.; Zhang, C. W.; Yang, Y. L.; Chu, Y. L.; L, S. B. Stability Test of W−Mn/SiO_2 Catalyst for Oxidative Coupling of Methane. *Petrochem. Technol.* **1995**, *24*, 293−298.
(114) Wang, X. L.; Zhang, J. N.; Yang, D. X.; Zhang, C. W.; Lin, J. Z.; Li, S. B. Oxidative Coupling of Methane over W-Mn/SiO_2 Catalyst in a Bench-Scale Stainless Steel Fluidized-Bed Reactor. *Petrochem. Technol.* **1997**, *26*, 272−277.
(115) Liu, H.; Wang, X.; Yang, D.; Gao, R.; Wang, Z.; Yang, J. Scale up and Stability Test for Oxidative Coupling of Methane over Na_2WO_4-Mn/SiO_2 Catalyst in a 200 Ml Fixed-Bed Reactor. *J. Nat. Gas Chem.* **2008**, *17*, 59−63.
(116) Chua, Y. T.; Mohamed, A. R.; Bhatia, S. Oxidative Coupling of Methane for the Production of Ethylene over Sodium-Tungsten-Manganese-Supported-Silica Catalyst (Na-W-Mn/SiO_2). *Appl. Catal., A* **2008**, *343*, 142−148.

DOI: 10.1021/acscatal.9b01585
ACS Catal. 2019, 9, 5912−5928